

IDENTIFICATION OF THE KEY LENGTH SCALES AFFECTING POOL BOILING PERFORMANCE PREDICTION FROM FINNED SURFACES

by

Maureen Winter

A Thesis

Submitted to the Faculty of Purdue University

In Partial Fulfillment of the Requirements for the degree of

Master of Science in Mechanical Engineering



School of Mechanical Engineering

West Lafayette, Indiana

May 2022

THE PURDUE UNIVERSITY GRADUATE SCHOOL
STATEMENT OF COMMITTEE APPROVAL

Dr. Justin Weibel, Chair

School of Mechanical Engineering

Dr. Shripad T. Revankar

School of Nuclear Engineering

Dr. Tom I. Shih

School of Aeronautics and Astronautics

Approved by:

Dr. Nicole L. Key

For my prince, Eric Alan Pio Karl II, on his birthday
Totus tuus, Maria, et ad majorem Dei gloriam!

ACKNOWLEDGMENTS

Special thanks to Dr. Justin Weibel, Purdue University, for his advice, encouragement, and help with every aspect of this thesis, and Dr. George Gogos, University of Nebraska-Lincoln, for teaching me how to conduct research and always believing in me. All my lab mates in the Cooling Technologies Research Center (CTRC) were also indispensable for the success of this research, whether helping me troubleshoot my facility or sharing their ideas and laughter. Gratitude is also due to all the members of the CTRC, without whose funding this research would not have been possible. I also acknowledge the National Science Foundation for support under the Graduate Research Fellowship Program (GRFP) under grant number DGE-1842166. Research and Development (R&D) is truly the center of Purdue, and I'm honored to have been a part of it for the past two years.

I could not have finished this thesis without the support of my friends and family who urged me to stay in grad school and reminded me to see the good around me. You've been with me every step of the way. Thank you, a thousand times over, and God bless you all.

TABLE OF CONTENTS

LIST OF TABLES	7
LIST OF FIGURES	8
LIST OF SYMBOLS	9
ABSTRACT.....	11
1. INTRODUCTION	12
1.1 Motivation.....	12
1.2 Boiling Enhancement Approaches.....	13
1.3 Objectives and Organization.....	14
2. LITERATURE REVIEW	15
2.1 Single Fin Boiling Performance Predictions.....	15
2.2 Fin Height and Spacing Effects during Boiling from Fin Arrays.....	17
2.3 Hypothesis.....	21
3. METHODS	23
3.1 Facility Description.....	23
3.2 Test Matrix.....	27
3.3 Test Procedure	28
3.4 Predicting Boiling Performance.....	29
4. RESULTS AND DISCUSSION.....	34
4.1 Boiling Visualizations.....	34
4.2 Boiling Curve Data	42
4.2.1 Height Effects	43
4.2.2 Spacing Effects	45
4.2.3 Summary of Experimental Data	47
4.3 Boiling Superheat Predictions.....	48
4.3.1 HFE-7100 Predictions	48
4.3.2 Water Predictions.....	51
4.3.3 CHF Predictions.....	52
4.4 Summary of Results.....	53
5. CONCLUSIONS AND FUTURE WORK.....	55

5.1	Conclusions.....	55
5.2	Future Work.....	56
APPENDIX A. VERIFYING POOL BOILING CONDITIONS		58
APPENDIX B. REMAINING WATER BOILING CURVES.....		60
REFERENCES		61

LIST OF TABLES

Table 3.1: Test matrix for testing the hypothesis.....	28
Table 4.1: Experimental and Predicted CHF Values	53

LIST OF FIGURES

Fig. 3.1: Experimental flow loop.	24
Fig. 3.2: Boiling chamber	25
Fig. 3.3: Sample with labelled dimensions of interest. Holes for thermocouple rakes are on the left side. The remaining thermocouples are inserted on the opposite side.....	26
Fig. 3.4: Heat flux and heat transfer coefficient as a function of superheat for (a) HFE-7100 and (b) Water. The power approximation is the correlation used to estimate the nucleate boiling regime heat transfer coefficient as a function of superheat.	31
Fig. 3.5: $h(\Delta T_w)$ functions from a flat surface used in the predictions (a) HFE-7100 (b) Water. Points marked with a green dot show the points used to define the transitional boiling regime.....	33
Fig. 4.1: Boiling regimes in HFE-7100 for 2.5 mm tall fins (a) H2.5-S8.5 (b) H2.5-S2.5 (c) H2.5-S1.0.	35
Fig. 4.2: Boiling regimes in HFE-7100 for 8.5 mm tall fins (a) H8.5-S8.5 (b) H8.5-S2.5 (c) H8.5-S1.0	37
Fig. 4.3: Boiling regimes in HFE-7100 for 1.0 mm tall fins (a) H1.0-S8.5 (b) H1.0-S2.5 (c) H1.0-S1.0.	38
Fig. 4.4: Boiling regimes in HFE-7100 on H0.5-S0.5 (a) Nucleate boiling regime (b) Partial film boiling regime. Full film boiling was not reached before CHF.	39
Fig. 4.5: Boiling regimes in water for 8.5 mm tall fins (a) H8.5-S8.5 (b) H8.5-S2.5 (c) H8.5-S1.0.	41
Fig. 4.6: Varying fin height in HFE-7100 at a constant 2.5 mm spacing.	44
Fig. 4.7: Varying fin height in water at a constant 8.5 mm spacing.	44
Fig. 4.8: Effects of spacing on fins in HFE-7100 (a) Spacing of 8.5 mm (b) Spacing of 1.0 mm and H0.5-S0.5	46
Fig. 4.9: Effects of spacing on fins in water, height at 8.5 mm with H2.5-S2.5 and H1.0-S1.0 ..	47
Fig. 4.10: Example of a boiling curve prediction for H2.5-S8.5 in HFE-7100.	49
Fig. 4.11: Predicted superheat versus experimental superheats in HFE-7100 (a) Samples with both height and spacing above L_b (b) Samples with height or spacing at or below L_b	50
Fig. 4.12: Predicted superheat versus experimental superheats in HFE-7100 (a) Samples with both dimensions at or above L_b (b) Samples with height or spacing below L_b	52

LIST OF SYMBOLS

Greek

σ	Surface tension [N/m]
ρ	Density [kg/m ³]
μ	Dynamic viscosity [Pa s]
α	Thermal diffusivity [m ² /s]
$\varepsilon\sigma(T_{abs}^4 - T_{sur}^4)$	Radiation effects term [W/m ²]
ν	Kinematic viscosity [m ² /s]
β	Expansion coefficient, [1/K]

Latin

A_{base}	Total base area of the sample [m ²]
A_{space}	Area of the space between fins [m ²]
C	Experimentally determined constant [W/m ² K ⁿ]
D	Diameter of a circular pin fin [m]
$\frac{d^2T}{dx^2}$	Change in the temperature gradient [K/m ²]
dw	Segment width [m]
g	Gravitational constant [m/s ²]
H	Fin height [m]
h	Heat transfer coefficient [W/m ² K]
h_{fg}	Latent heat [J/kg]
k	Thermal conductivity [W/mK]
L	Fin width [m]
L_b	Capillary length scale, $\sqrt{\frac{\sigma}{g(\rho_l - \rho_v)}}$, [m]
n	Experimentally determined exponent [unitless]
N_{fin}	Number of fins on the heat sink [#]
N_{space}	Number of spaces in the finned heat sink [#]
q''	Heat flux [W/m ²]

S	Fin spacing [m]
t	Fin thickness [m]
T	Temperature at a given point on a fin [K]
ΔT	Superheat [K]
w	Segment location along fin wall [m]
x	Location along a fin [m]

Subscripts

b	At base
fin	Single fin
$film$	Film boiling
in	Into a segment
$cond$	Conduction
$conv$	Convection
l	Liquid phase, property taken at saturation conditions
max	Taken from the last point before the CHF of the flat surface
min	Taken from the first point after film boiling begins
NB	Nucleate boiling
NC	Natural convection
out	Out of a segment
tot	Total
v	Vapor phase, property taken at saturation conditions
w	At location w

ABSTRACT

Heat sinks have the capability of increasing operating heat flux limits for improved thermal management in the immersion cooling of electronics using dielectric fluids. However, even for arrays of simple, straight fins, the generation of vapor between and along fins during pool boiling lead to performance effects that are not well understood. Further investigation of the heat-flux-dependent variation of boiling modes that can manifest along the fin height is required. Although methods for the prediction of fin boiling heat transfer exist that incorporate a variable heat transfer coefficient determined from a flat surface, they have been developed and assessed for single, isolated fins under the assumption that the sides of the fin at any location behave like that of a flat surface. As a result, when applied to fin arrays, these methods may not always be accurate for the full range of heat flux operation along boiling curve up to the critical heat flux, due to the fins interfering with each other when arranged in arrays of differing spacing and height. To establish when the fins in an array can be described as isolated and having the flat surface boiling behavior, pool boiling experiments are performed using copper heat sinks in two fluids with vastly different properties: HFE-7100 and water. The spacing and height of the longitudinal fins are varied across a range from much larger to less than half of the scale of the capillary length scale of both fluids, L_b . High-speed visualizations enable the identification of different boiling regimes to identify correspondence between flow observations and the boiling performance, such as when there is bubble confinement from fin interference. Trends in the pool boiling data are also compared, noting changes in superheat at various heat fluxes to establish when fin height or spacing affects boiling behavior. The experimental boiling performance is compared to predictions developed assuming isolated fins so as to identify the spacings and heights for which the fin arrays follow this behavior. Overall, the data from both fluids strongly support a hypothesis that L_b is the key length scale. Heat transfer from fin array heat sinks with heights and spacings above L_b are shown to be accurately predicted in both fluids. However, spacings smaller than L_b lead to bubble confinement which affects the superheat, particularly at low heat fluxes, while heights shorter than L_b are unable to support multiple boiling regimes along the fin sidewall. This work identifies the capillary length as the key length scale at which confinement and height effects need to be considered for accurate predictions of immersion cooling applications.

1. INTRODUCTION

1.1 Motivation

Efficient electronics cooling is of critical importance in today's increasingly digital, interconnect world. As computer processing units consume more power and decrease in size, it is increasingly difficult to dissipate the heat generated from such a small area. Advanced laser systems, personal electronics, and electric vehicles are all examples of power-dense devices where insufficient heat rejection limits their performance, whether for computational efficiency or charging speed. Data centers in particular require incredible amounts of energy dedicated to electronics cooling; in 2019, data centers alone used 3% of the electricity produced globally, around 40% of which was used for cooling, and that amount continues to rise [1]. Air cooling is still the typical cooling strategy in data centers due to relatively low operating costs [2]; however, because electronics require a specific temperature range to operate efficiently and reliably, air cooling is fast becoming infeasible for increasingly power-dense next generation data centers. New methods are required to dissipate high heat fluxes within electronic systems

One efficient method for dissipating heat is through two-phase immersion cooling. In two-phase immersion cooling, the heated electronics are directly in contact with a fluid at its saturation temperature, initiating a phase change on the surface as power increases. The phase change occurs at a constant fluid saturation temperature, and as the heat generated by the electronic device varies in time, the amount of vapor formed at the boiling surface can simply increase or decrease accordingly. Buoyancy forces then passively lift the vapor from the surface and allow for this excellent heat transfer process to occur passively, without requiring pumping of the coolant in the cooling process. Heat transfer coefficients orders of magnitude greater than single phase cooling are possible. However, the implementation of immersion cooling of electronics is still being explored. Several practical concerns include fluid-materials compatibility, leakage, and overall amount of coolant as summarized in [1]. One fundamental concern of using direct immersion cooling for electronics is that the necessary dielectric fluids have low critical heat fluxes (CHF). Considered a failure condition in boiling heat transfer, CHF is the maximum heat flux that can be sustained before a vapor film blankets the surface, preventing liquid from reaching the surface to change phase. The result is a drastic decrease in the heat transfer coefficient accompanied by a

sudden increase in temperature, often severe enough to damage the electronics. For candidate dielectric working fluids, CHF occurs on the order of only $\sim 20 \text{ W/cm}^2$ from a smooth, flat surface. Boiling enhancements are necessary to increase the critical heat flux of dielectric fluids and implement them for two-phase immersion cooling of electronics.

1.2 Boiling Enhancement Approaches

There are multiple enhancement approaches focused on micro- and nanoscale surface features. One technique is to roughen the surface. This provides more nucleation sites, promoting boiling spread uniformly across the heated surface at lower superheats than smooth surfaces [3]. While the addition of surface roughness is able to lower surface superheats at a given heat flux by over 10 K in dielectric fluids, predicting the amount of enhancement is notoriously difficult [4]. Enhancement can also be achieved by changing the wettability of the surface. Surfaces with increased wettability promote liquid flow to the surface beneath forming vapor bubbles, thereby delaying CHF [5]. Nonwetting coatings favor vapor nucleation from the surface at lower superheats leading to dense coverage of the surface [6]; however, CHF is severely reduced. Recent experiments with alternating hydrophilic and hydrophobic regions [7, 8] or parahydrophobic surfaces that intermix these wetting characteristics [9] have been quite promising, lowering the superheat yet retaining high CHF. Microporous coatings and layers added to boiling surfaces also show significant enhancement. Liquid is drawn into these porous coating on the heated surface by capillary forces to displace the generated vapor [10, 11]. Nanoscale structuring of surfaces can offer various effects such as decreasing the nucleate boiling superheat or improved wettability [12, 13]. Further discussion of pool boiling enhancement techniques is given in [14–16]. However, an overarching observation is that microscale coatings and nanoscale enhancements risk deterioration over time and lack the longevity for current implementation.

Macroscale enhancement using extended surfaces (i.e., fins) can reliably improve the boiling heat transfer performance of dielectric fluids and increase the critical heat flux. By increasing the amount of area where phase change can occur through the use of a heat sink, the overall heat flux can be lowered significantly for a given power input. Moreover, the extended area can support multiple boiling regimes at once. Even if film boiling occurs at the base surface of the heat sink, this local dryout can be offset by activating efficient nucleate boiling further up the sides of the fins [17–21]. This delays CHF and enables heat dissipation levels far above that of a flat surface.

Further enhancement is obtained by combining microscale enhancement with macroscale heat sinks, but there is little research in this area [19, 22, 23].

Before heat sinks can be readily deployed for immersion cooling applications, it is necessary to improve the accuracy of predictions for boiling from extended surfaces. Important and fundamental design questions related to heat sinks have been neglected in the excitement of micro- and nano-enhancement research. For example, the desirable feature size for spacing between extended surfaces, or length necessary for fins to delay CHF after dryout of the base, remain unclear. Of particular importance is determining the accuracy of methods for incorporating temperature- and regime-dependent boiling heat transfer coefficients in fin analyses for varying fin dimensions. Nucleate boiling offers significantly increased heat transfer capability when compared to film boiling or natural convection, and so when multiple regimes are present, a complex distribution of the heat transfer coefficient must be considered along the fin. The design optimization techniques developed for single phase heat sinks assume uniform heat transfer coefficients and are not viable.

Currently, the established method to incorporate a spatially variable boiling heat transfer coefficient in heat sink performance predictions is by assuming boiling performance correlations obtained from flat surfaces can be borrowed to predict the performance of vertical fins or other structures. In other words, boiling from all sides of the fin structures is assumed to behave like a flat surface, regardless of potential orientation or confinement effects due to close spacing of multiple fins. Determining height and spacing length scales for this to be a reasonable assumption is necessary before heat sinks can be designed and optimized for boiling.

1.3 Objectives and Organization

This thesis seeks to answer the question of when fins can be treated as independent, ultimately determining minimum length scales for spacing and height required for application of the flat surface boiling behavior to the fin structure for heat transfer analysis. The thesis is organized as follows. Chapter 1 provides the motivation and background. Chapter 2 is the literature review that leads to the development of the specific research hypothesis. Chapter 3 describes the methods, both for the experiments and the analytical predictions. Chapter 4 presents the results. Lastly, Chapter 5 draws the final conclusions regarding the hypothesis and suggests future work related to this thesis.

2. LITERATURE REVIEW

2.1 Single Fin Boiling Performance Predictions

While fin arrays have been developed intuitively for boiling applications such as heat exchanger tubes as early as the 1960s [21], methods for predicting their performance for purposes of shape/dimension optimization were developed from examining boiling from a single fin. Haley and Westwater [24] performed an analysis for boiling from a copper fin in R-113 or isopropanol. In order to optimize the fin shape, they performed a one-dimensional heat transfer analysis on a cylindrical fin to predict the fin heat transfer. Boundary conditions of convection at the tip and a fixed temperature at the base were applied to the following governing equation.

$$\frac{d^2T}{dx^2} = \frac{4}{k(T)D} (h(T)\Delta T + \varepsilon\sigma(T_{abs}^4 - T_{sur}^4)) \quad (1)$$

where T is the temperature at location x on the fin, D is the diameter of the circular cross-section fin, k is the thermal conductivity as a function of fin temperature, and $\sigma\varepsilon(T_{abs}^4 - T_{sur}^4)$ incorporates radiation effects. The most relevant term is $h(T)$, the boiling heat transfer coefficient as a function of the surface temperature. The nucleate boiling heat transfer coefficient increases significantly with surface temperature and other boiling regimes have vastly different heat transfer on temperature. In particular, as heat flux increases to the fin, it has been observed that film boiling can occur partially over the fin base while nucleate boiling continues along the fin sides and the top of the fin is still in natural convection. This behavior leads to dramatically different, temperature- and regime-dependent heat transfer coefficients along the fin. Haley and Westwater [24] solved the problem of variable heat transfer coefficient by assuming that boiling from the sides of the fin surface would have the same $h(T)$ function as a flat boiling surface, regardless of orientation. By performing boiling tests on a horizontal surface, they could determine the $h(T)$ function that could then be used with Equation (1) to iteratively solve for the total heat flux and the final temperature distribution in the fin. Their predictions show overall good agreement for a single cylindrical fin, successfully predicting the varying slopes of the boiling curve and the CHF.

After establishing that the boiling performance of single fins could be predicted using $h(T)$, from a flat surface, Haley and Westwater [24] optimized the profile of the cylindrical fin for

minimum volume. Because nucleate boiling has the highest heat transfer coefficient, the idea was to maximize the surface area in that regime, while minimizing area where the less effective film boiling and natural convection would occur. The resulting fin was turnip-shaped, with the widest point where the calculated temperature distribution indicated there would be nucleate boiling. Later, Cash et al. [20] simplified the shape to make it easier for machining, resulting in a final fin shape formed from two conical sections. While the heat transfer in this simplified shape was significantly underpredicted due to turbulence effects, the approximate optimum fin shape outperformed regular cylindrical fins, indicating the value of the optimization.

Lai and Hsu [18] also examined heat transfer predictions for boiling on single fins. Taking a simplified approach, they focused on the length of the boiling regimes, incorporating average heat transfer coefficients for film, transition, and nucleate boiling as well as natural convection. Then, using the boiling incipience superheat and the heat flux into the fin, they could predict the length of each regime without numerical discretization along the fin length. While these predictions of final temperature distribution were not as accurate as the method above, the benefits of decreased computational expense allow them to provide an initial estimate for a more rigorous computational method.

Later, Lin and Lee [25] built on Lai and Hsu's [18] work by performing an analytical stability analysis to further examine the effects of varying regimes on a single pin fin. Taking a separate power law for the heat transfer coefficient dependence on temperature for film, transition, and nucleate boiling, they iteratively solved steady-state, one-dimensional fin analysis to determine the temperature distribution. Cases with one, two, or all three regimes were studied. By then perturbing the temperatures in the steady solution, it was possible to analyze when the boiling was stable. They concluded their analysis by proposing that the ideal fin would have the final fin tip temperature just slightly below the temperature where CHF was reached on the flat surface, and the fin length should be selected accordingly.

Fantozzi et al. [26] further examined heat transfer predictions, focusing on showing that one-dimensional fin analysis is accurate. Using a single longitudinal fin made from aluminum, they placed thermocouples along the thin side to record the temperature profile in the fin during pool boiling in HCFC141b. From this temperature profile, they observed that CHF for a single fin occurred when the temperature at the tip of the fin reached the CHF superheat of the plane surface, confirming similar trends noticed by Haley and Westwater [24]. Fantozzi et al. [26] also calculated

an average heat transfer coefficient that minimized error between the measured temperature profile and established power laws. The average heat transfer coefficient was then used in numerical simulations of conduction through the fin to predict the performance of an array of longitudinal fins spaced 2 mm apart, with the simulations showing agreement within 10% of the experimental values. Overall, their conclusion from the experiments was that one-dimensional fin analysis, coupled with the plane surface superheat at CHF, and use of the average heat transfer coefficient was sufficient to determine finned heat sink performance.

However, Fantozzi et al. [26] noticed that the predictions, particularly of CHF, worked best for the longest fins tested. There was less agreement for shorter fins. They also observed that a single fin with total area less than the plane surface could not reach a steady surface temperature once the base around the fin was in a film boiling condition, but an array of short fins could, something not captured by the predictions. From these observations, it is clear that fin height and total surface area affect the overall heat transfer performance in ways that are not captured by models assuming they all fins act independently.

2.2 Fin Height and Spacing Effects during Boiling from Fin Arrays

Fin array height and spacing effects are clearly demonstrated in the experiments of Mudawar and Anderson [22]. Using Haley and Westwater's [24] approach of assuming that the fin sidewalls boil with the same performance as an isothermal flat surface, irrespective of orientation, 2D numerical models of the fin heat transfer were compared with experimental results for copper pin fins placed horizontally in FC-72 and FC-87. The numerical solutions had good agreement with the experiments for single fins of varying height, with both the experiments and the predictions indicating that the overall boiling curves should be the same until near CHF, when the longer fins have better performance. They also predicted the performance of two fin arrays, one with four fins (2×2 array) and the other with nine (3×3 array), all spaced at 0.6 mm. The 2×2 array had good agreement with the predictions for the entire curve, however, the prediction for a 3×3 array with the same spacing did not capture the trends of the boiling curve as accurately. This is attributed to confinement effects that become more important when some fins are in the center.

Mudawar and Anderson [22] also demonstrated predictions for macroscale fins with microscale features to further enhance the heat transfer capabilities. First, they tested a horizontal surface covered in microgrooves in the form of 0.5 mm tall studs or longitudinal fins, chosen for

the enhancement characteristics presented in [27]. From these experiments, the boiling $h(T)$ for the micro-enhanced surfaces could be determined. This function was then used with 2D numerical models to predict the performance of 12.192 mm long, 10 mm diameter pin fins covered in the same microstructures, grooved either axially, radially, or in both directions. There was excellent agreement, particularly for axial and radial micro-grooves, and the micro-studded pin fin had over twice the CHF of the flat micro-studded surface.

Rainey and You [19] also examined varying height for plain and microporous coated pin fins. Using an array of square $1 \times 1 \text{ mm}^2$ pin fins with a fixed spacing of 1 mm in FC-72, they varied the height from 0 to 8 mm and examined the effects, using fin efficiency to directly compare the plain and microporous structured surfaces. Similar to the observations of Mudawar and Anderson [22], there is general agreement between the samples' boiling curves at low heat fluxes, regardless of the fin height, particularly for the microporous coated fins. Only the portion of the curve near CHF is affected by the height changes. This work also used an average heat transfer coefficient determined by numerically solving the overall fin surface efficiency equations at each heat flux and superheat to perform a 1D fin analysis and estimate the temperature at the tips of the fin. From the temperature analysis, it was clear that for non-coated fins, the temperature at the tip of the longest fins, just before CHF, was slightly lower than the superheat required for nucleate boiling, indicating that nucleate boiling heat transfer does not occur there despite the available area. This was confirmed by the fact that the plain finned surfaces showed a decrease in overall surface efficiency for the longest fins. From this, they determined that the maximum height for efficiency improvements for this fluid/surface combination was around 5 mm, both because of the low superheat at the tip. They also noticed that the tall fins had bubble departure interference, delaying rewetting and increasing overall superheat, ultimately leading to partial dryout at the base of the fins. Looking at the microporous covered fins, the estimated superheat at the tips just before CHF was around 19 K, well over the superheat required for nucleate boiling allowing, allowing high heat transfer coefficients over the whole fin. These observations explained why the plain fins followed Zuber's flat-surface CHF prediction [28] for short heights, while the microporous-coated fins showed good agreement with predictions regardless of height.

Guglielmini et al. [29] examined arrays of square, copper fin arrays with two different spacings, 0.4 mm and 0.8 mm. Galden HT55 was the working fluid, and the samples were tested in the horizontal and vertical orientation at three different pressures. Key observations were that

for both varying pressure and changes in orientation, the boiling curves for each sample converged at high heat fluxes for each testing case, indicating little impact from pressure or orientation. The two spacings also converged at high heat fluxes for both orientations. They reasoned that the highly wetting properties of the working fluid negated any orientation or spacing effects. In addition, they noticed that at low heat fluxes, the horizontally oriented fins showed more uniform boiling, leading to a lower superheat. Overall, the smaller spacing had slightly better heat transfer performance, with more active nucleation sites. However, the increase in performance was not proportional to the increase in boiling area resulting from more fins at smaller spacing. This is most likely because the fins were spaced overly close and impeded bubble departure. They concluded that spacings below the bubble departure diameter of the fluid could interfere with area enhancement.

Klein and Westwater [30] attempted to determine minimum spacing required for all fins to act independently of each other. Experiments were conducted in R-113 and water on round copper fins oriented horizontally in a unique test setup with the fins set into grooves that allowed changeable spacing. While the flexibility of the setup allowed spacings from touching to 25.4 mm to be tested, each row of fins was separated by a constant distance of over 9.5 mm, limiting conclusions for a full array, where spacing in both directions could constrict vapor. Moreover, particularly for R-113, it was noticed that there was boiling beneath the fins in the grooves, which could also interfere with spacing effects. To mitigate the concern of constant row spacing, tests were also conducted with flat plates acting as longitudinal fins in R-113 to confirm the minimum spacing requirement of 1.6 mm for independent fins. For tests conducted in water, it was observed much more vapor billowed around the sides rather than between the fins, limiting the spacing conclusions when only one direction was being tested. However, when baffles were installed to constrict the vapor going around the fins, the minimum spacing required for independent fin performance was found to be the same as for R-113, namely 1.6 mm. Note that water was not tested with longitudinal fins. Ultimately, while their work shows that there is a minimum spacing for fins boiling in fluids to act independently, the boiling beneath the fins and lack of spacing effects in both directions make the final conclusions difficult to apply in other scenarios.

The overall effects of height and spacing are well summarized in the work of Yu and Lu [31]. Using copper fins in FC-72, spacings of 0.5, 1, and 2 mm were tested with varying fin lengths of 0.5, 1, 2, and 4 mm. At the largest spacing, fins taller than 0.5 mm had boiling curves essentially overlapping each other until near CHF, where the 4 mm tall fins outperformed the others. As

spacing decreased, there was less agreement in the curves, with 0.5 mm spacing showing the shortest fins performing the best at lower heat fluxes. While confirming the height effect observations from [19, 22], the spacing component is of key interest as well. When the spacing is too small, the boiling curves are no longer independent of height at low heat fluxes. Lastly, they also noticed that tall fins and closer spacing inhibit bubble departure, similar to what was seen by Rainey and You in [19]. Overall, the fin array capable of withstanding the highest heat fluxes had the tallest and most closely spaced fins, achieving a CHF almost five times greater than the plain surface.

Experiments in water at low pressure verify the trends for height and spacing effects. McGillis et al. [32] performed experiments in water at 9 kPa for copper fins of varying height and spacing. They noticed that for fins at or longer than 2.54 mm, the boiling curves matched each other, even when spacing changed slightly. Height experiments were not run to CHF due to the extremely high surface temperatures reached prior to CHF when using water, and so high heat flux boiling curve performance could not be determined. They also varied fin thickness, demonstrating no change in the boiling performance for samples with a thickness of 0.69 mm versus 1.78 mm. Further experiments varying the spacing between fins demonstrated that smaller spacing decreased the superheat for a given heat flux, increasing overall performance, but for spacings at or larger than 1.59 mm, the performance was identical at low heat fluxes. When the experiments were run to CHF for 2.54 mm fins spaced at 1.59 mm and 2.54 mm, the smaller spaced fins demonstrated greater heat transfer capability. Their conclusions were that the smaller gap allowed for more boiling surface area (more fins) and also confined the liquid, promoting more nucleation up the sides of the fins. Overall, there was confirmation that a minimum height and spacing exists above which boiling performance no longer changes.

Abuaf et al. [17] also performed pool boiling experiments on finned surfaces at low pressures, specifically with the goal of applying the predictive methods of [24]. The boiling surface had copper 1.6 mm square pin fins with a height of 3.2 mm and 1.6 mm spacing. These were tested in R-113 at pressures ranging from 0.037 to 0.89 atm. By examining the literature, they compiled $h(T)$ correlations into a function for R-113 on a flat surface at atmospheric pressure and applied a 1D fin analysis with successive overrelaxation in order to determine the heat flux through the finned structures at a given superheat. At lower pressures, they modified the correlations for $h(T)$

accordingly. Conclusions showed that for pressures near atmospheric, the predictions held quite well, both for boiling curve trends and CHF, though at low pressures they no longer agreed.

There have also been a few experiments with fins of varying shape. Park and Bergles [33] compared the boiling enhancement of copper fins extending from a plate to the boiling enhancement of cylinders cut into a plate. Both were tested in a horizontal orientation in R-113. Ultimately, it was shown that holes of 0.71 mm diameter outperformed the fins, providing a CHF approximately nine times that of the flat surface. Mudawar and Anderson [23] examined varying dielectric fluids at different pressures and subcooling temperatures as well as the effects of fin shape. Their overall goal was to reduce the boiling incipience temperature and increase the CHF. While spacing and height were not varied, the fins tested provided an interesting example of multi-scale enhancement. Pyramids and squares with 0.5 mm long studs wrapping around the primary fin spaced 0.3 mm apart provided essentially smaller fins on the larger fin core. These were compared with large cylindrical fins spaced 0.6 mm apart, a distance similar to the capillary length scale of the fluid. When the bubbles formed on the 0.5 mm long studs, they nucleated on the underside first, working outwards through the grooves. This confinement ultimately caused sudden bubble nucleation further up on the fin than the base heat would suggest, resulting in nonuniform boiling and undesired temperature overshoots. The cylindrical fins, meanwhile, provided uniform boiling that gradually rose along the fin height with increasing heat flux, showing that fins of smooth cross section allowed for more uniform boiling and less temperature overshoot than studded square fins or pyramids. Overall, the experiments of [23, 33] indicate that vapor confinement must be taken into consideration when attempting to design a heat sink.

2.3 Hypothesis

All these results from the literature point to specific length scales for the fin array height and spacing that determine whether vapor is confined. Vapor confinement challenges the primary assumption of predictive methods for boiling from heat sinks, namely, that flat surface behaviors can be used to predict the fin sidewall performance. Since these predictive methods were developed and validated only using single fins, it is clear that a minimum spacing is required for accurate boiling curve predictions. Otherwise, the fins will interfere with each other, causing bubble confinement [29–32]. There is also the question of very tall fins having the potential for interference, as stated in [19, 31]. Both of these aspects are not captured by the single-fin model

proposed by Haley and Westwater [24]. After examining the literature above, this thesis poses a hypothesis based on the capillary length scale of the fluid (L_b).

$$L_b = \sqrt{\frac{\sigma}{g(\rho_l - \rho_v)}} \quad (3)$$

where σ is the surface tension of the fluid, g is the acceleration due to gravity, and ρ_l and ρ_v are the density of liquid and vapor, respectively. If fins are spaced further apart and taller than L_b they will in fact behave as single fins, and a flat surface can be used to determine the heat transfer coefficient as a function of temperature. If they are shorter than or spaced closer than L_b , the assumption that they act as single fins will not hold, and there will be a different boiling behavior due to bubble confinement. To evaluate this hypothesis, pool boiling tests are conducted in two fluids with drastically different L_b , HFE-7100 and water.

3. METHODS

3.1 Facility Description

All experiments were conducted in a pool boiling chamber at atmospheric pressure using the flow loop shown in Fig. 3.1. The facility has been significantly modified since its original construction for performing two-phase jet impingement experiments [34] and subsequent additional experiments in [35–37]. The working fluid (water or HFE-7100) begins in a reservoir where it is maintained at the saturation temperature and degassed with three immersion heaters (Watlow). Three Graham condensers (Ace Glass, 4071-12), cooled in series with a water-glycol chiller (ThermoCube, 10-400-1C-1-CP), allow non-condensable gases to escape from the reservoir. A magnetic gear pump (Micropump, GD-M35.PF5S.E) pumps fluid through the system and is monitored by a Coriolis flow meter (Micro-Motion, CMFS015M). There is a liquid-to-air heat exchanger (Lytron, AS06-08G01SB) with the fan speed controlled to ensure that the fluid is sufficiently cooled and there is no vapor in the pump. A bypass loop with a needle-controlled valve allows finetuning of the flow rate and prevents pressure buildup, and a second subloop contains 15 μm filters (Swagelok, SS-8F-K4-15) used only during pre-test degassing. The fluid then flows into the polyether ether ketone (PEEK) testing chamber before returning to the reservoir. Polycarbonate viewing walls with even backlighting (Micromation, BT200100-WHICH) allow clear viewing of the tests with a high-speed camera (Phantom Vision Research, VEO710L).

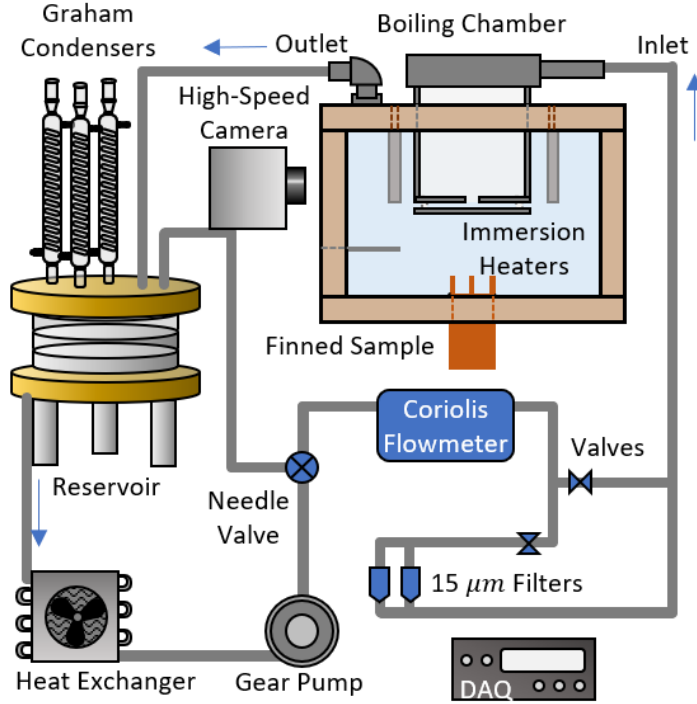


Fig. 3.1: Experimental flow loop.

The fluid enters the test chamber through a polycarbonate plenum, shown in Fig. 3.2. The plenum is topped with a polyamide-12 (PA 12) flow distributor, while at the bottom, a polycarbonate plate deflects the flow radially through 3.17 mm wide gap. The larger area of $\sim 750 \text{ mm}^2$ at this gap ensures that the liquid flow has a small velocity, such that the fluid in the testing chamber is essentially quiescent and can be considered pool boiling. Verification of the pool boiling condition across multiple fluid flow rates is given in Appendix A. In order to keep the fluid in the chamber at saturation conditions, two immersion heaters (Watlow) are inserted into the boiling chamber. The sidewall thermocouple (Omega, TJ36-CPSS-18-12) verifies the fluid is at saturation. The immersion heaters connect to a variable power source (Superior Electric, 3PN116C) and power is gradually decreased as the sample heat flux increased to generate a consistent overall amount of vapor exiting the chamber. A pressure tap (Omega, PX302-XXGV) inserted in the bottom of the chamber ensures that the test remains at atmospheric conditions.

Samples, shown in Fig. 3.3, are fabricated from copper using additive manufacturing (Markforged MetalXTM). Key dimensions are the height of the fins (H), the spacing between fins (S), the fin thickness (t), and the width of the fin (L). Twelve holes evenly placed in the bottom of the sample fit 1 in. long, 60 W cartridge heaters (Watlow). Each sample has three thermocouple

rakes (Omega, TJ36-CPIN-116-12): front, back, and center. These allow area-averaged heat flux and surface temperature extrapolation via a linear regression model assuming 1D heat flow through the sample. The 1D heat flow assumption is reasonable because of the high thermal conductivity of the copper (nominally 350 W/mK) and the low heat loss for similar samples, as assessed using a numerical conduction simulation (ANSYS Fluent) of the assembly previous performed in [37]. The four thermocouples in the center rake are spaced 2.54 mm apart starting 2.19 mm from the top of the sample. The front and back rakes contain two thermocouples 2 mm from the front and back edge and even with the top and bottom thermocouples in the center rake. Prior to insertion into the sample, each thermocouple is coated with thermal paste (Omega, Omegatherm 201) to ensure complete contact and consistent measurements, and all thermocouples are referenced to a dryblock icepoint chamber (Omega, TRCIII)..

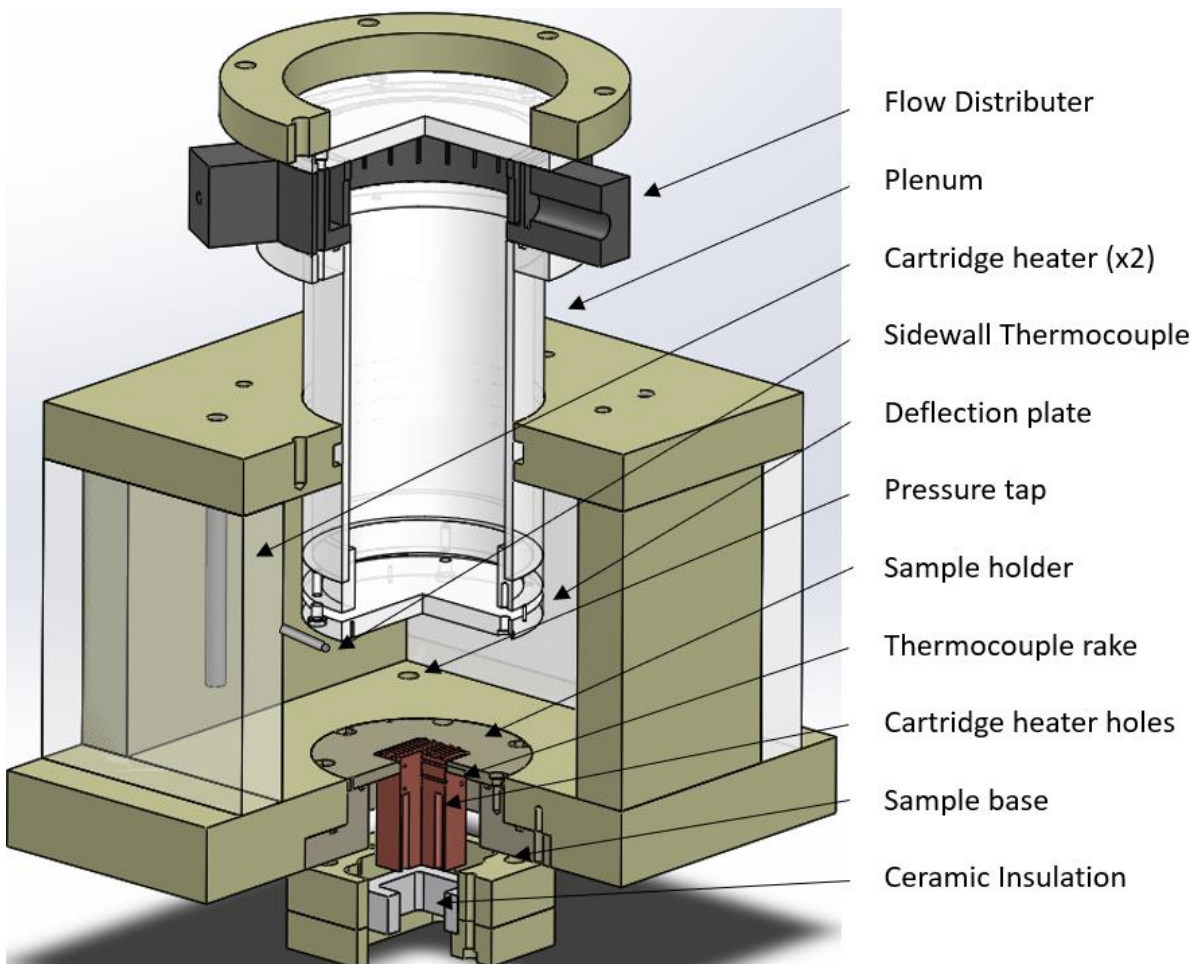


Fig. 3.2: Boiling chamber

All samples have a 20×20 mm base with longitudinal fins of varying height and spacing. Longitudinal fins were chosen to allow clear viewing of the boiling between and on the fins. For testing, the sample is placed in a PEEK holder and leveled using the adjustable screw and spring base before being sealed (Dow, Q3-6611), as shown in Fig. 3.2. A ceramic block is placed between the sample and the base to insulate the hot sample and prevent it from melting the PEEK. Lastly, two O-rings, one between the sample holder and the base and one between the chamber and the base, prevent leaks around the sample.

An uncertainty analysis was conducted by analyzing the error in the block temperature gradient using the methods in [38] and the stated accuracy of the thermocouples ($\pm 1\text{K}$ or 0.75% of the thermocouple reading, whichever is greater). The results showed an uncertainty in the area averaged surface temperature between 1.0 K and 1.5 K for all heat fluxes tested in HFE-7100. In water, the uncertainty in the area averaged surface temperature was slightly greater, between 1.2 and 2.2 K for all heat fluxes tested. Uncertainty in the calculated heat flux for HFE-7100 was $\sim 3.8\text{ W/cm}^2$ at a heat input of 12 W/cm^2 and $\sim 4\text{ W/cm}^2$ near a heat input of $\sim 100\text{ W/cm}^2$. Higher heat inputs tested in HFE-7100 had greater uncertainties, with the largest uncertainty $\sim 4.5\text{ W/cm}^2$ at a heat input of $\sim 130\text{ W/cm}^2$. For water, the uncertainty in the calculated heat flux ranged from $\sim 3.8\text{ W/cm}^2$ at 25 W/cm^2 heat input and $\sim 7\text{ W/cm}^2$ at a heat input of 300 W/cm^2 .

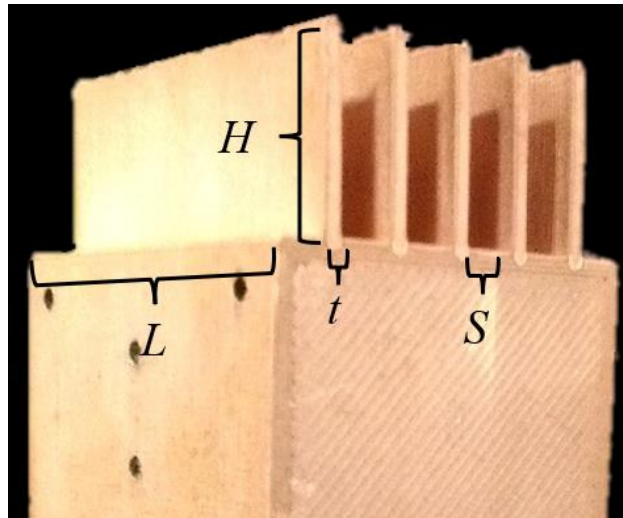
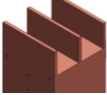
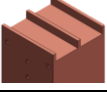
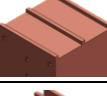
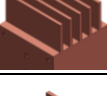
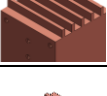
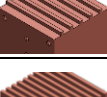
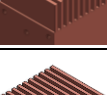
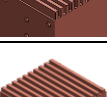
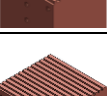



Fig. 3.3: Sample with labelled dimensions of interest. Holes for thermocouple rakes are on the left side. The remaining thermocouples are inserted on the opposite side.

3.2 Test Matrix

In order to test the hypothesis, samples were fabricated with height (H) and spacing (S) dimensions based on the capillary length (L_b) of water and HFE-7100. To analyze height and spacing much larger than the suspected key length scale, dimensions of 8.5 mm were chosen, ~ 3 times the L_b of water and much larger than the L_b of HFE-7100. Intermediate 2.5 mm dimensions were used as a length scale larger than the L_b of HFE-7100 and on the same order as the L_b of water. Small 1.0 mm dimensions were used to test samples at a scale smaller than the L_b of water and on the same order as the L_b of HFE-7100. Lastly, a single 0.5 mm height and spacing sample was tested in HFE-7100 to show the effects of dimensions smaller than the L_b of HFE-7100. All fins were longitudinal across the base of the sample and were 1 mm thick (t). Since $t=1$ mm thickness is less than or comparable to the L_b of water and HFE-7100 respectively, it was assumed that fin thickness effects would be minimal with regards to the hypothesis, enabling conclusions to be isolated to fin height and spacing effects. Additionally, the thickness is twice as large as the $500\text{ }\mu\text{m}$ minimum print size, allowing consistent samples. The full sample test matrix for HFE-7100 is shown in Table 3.1. The two parts of the sample name denote the height of the fins ($H \times x$) and the spacing between the fins ($S \times x$) in mm. Samples also tested in water are indicated with an asterisk*.

Table 3.1: Test matrix for testing the hypothesis

Sample (Height-Spacing)		Parameter		
		Total Boiling Area to Footprint Ratio	H/L_b Ratio	S/L_b Ratio
H8.5-S8.5 *		3.55	8.5	8.5
H2.5-S8.5 *		1.75	2.5	8.5
H1.0-S8.5 *		1.30	1.0	8.5
H8.5-S2.5 *		5.25	8.5	2.5
H2.5-S2.5 *		2.25	2.5	2.5
H1.0-S2.5		1.50	1.0	2.5
H8.5-S1.0 *		9.50	8.5	1.0
H2.5-S1.0		3.50	2.5	1.0
H1.0-S1.0 *		2.00	1.0	1.0
H0.5-S0.5		1.65	0.5	0.5

*: Tested in water and HFE-7100

3.3 Test Procedure

Before beginning each test, the working fluid is degassed for at least 2 hr in the reservoir and the sample is gradually heated to vigorous boiling at $\sim 15 \text{ W/cm}^2$ for HFE-7100 or $\sim 100 \text{ W/cm}^2$ for water to ensure test repeatability and similar initial conditions. The filtering subloop is also opened during this degassing period in order to remove any contaminants from the fluid. When degassing is finished, the filtering flow loop is closed and the flow rate is adjusted to the testing

conditions, approximately 250 mL/min. The sample is then allowed to cool to steady state to take the first data point, with steady state defined as when the calculated surface temperature of the sample changes less than 1 K/hr. Once steady state is reached, a high-speed video is taken of the boiling surface, and data for each point is recorded for 2 min at 0.5 Hz then averaged to determine the surface temperature and heat flux through the sample. After recording each data point, the sample input power is increased in steps of ~10-24 W for HFE-7100 or ~100-150 W for water and allowed to stabilize at each power. For both water and HFE-7100, at high heat fluxes, there are cases where the surface temperature is either very gradually increasing or decreasing with no indication of leveling to a steady state condition in a reasonable amount of time (<2 hr). In these cases, a fixed time of 45 min was allowed to elapse before taking the next data point. Oscillations in the surface temperature about a steady reading also occurred at high heat fluxes, particularly for tall fins in HFE-7100, making it difficult to strictly follow the steady state criterion. For these points, data was taken when it was clear from transient temperature data that the surface temperature had levelled out to a steady value but was experiencing some oscillations from base film boiling.

Critical heat flux was the general stopping condition followed for all HFE-7100 tests, as signified during the experiments by large superheat increases and vapor completely covering the entire heat sink boiling area. One test, H8.5-S1.0, was stopped due to condenser overload from the amount of vapor generated. For tests with water, due to the increased saturation temperature (and thereby surface temperature) as well as concerns for damaging the facility if CHF was reached, tests were stopped when the surface temperature reached 50 K superheat. Two samples, H1.0-S1.0 and H1.0-S8.5, reached the CHF condition in water, while H8.5-S1.0 was stopped due to a cartridge heater failure at the high power.

3.4 Predicting Boiling Performance

All boiling curves were compared to predictions defined using a 1D fin analysis and variable heat transfer coefficient. A single fin was divided into small segments of length d_w and an energy balance was performed in each segment.

$$q''_{cond, in} = q''_{conv} + q''_{cond, out} \quad (4)$$

where

$$q''_{cond, in} = -k \frac{\Delta T_w - \Delta T_{w-1}}{dw} \quad (4a)$$

$$q''_{cond, out} = -k \frac{\Delta T_{w+1} - \Delta T_w}{dw} \quad (4b)$$

$$q''_{conv} = h(\Delta T_w) \Delta T_w \quad (4c)$$

where k is the thermal conductivity of the copper fin, 350 W/mK, ΔT_w is the wall superheat at the center of segment w , with -1 and +1 representing the centers of the segments above and below segment w , and $h(\Delta T_w)$ is the variable heat transfer coefficient as a function of wall superheat at w . The boundary conditions are the known temperature at the base of the fins (from the thermocouple rakes) and convection at the tip of the fin. Using the approach of Haley and Westwater [24], an additively manufactured flat copper surface was tested both in water and HFE-7100 to determine $h(\Delta T_w)$ for the nucleate boiling regime, resulting in a power correlation.

$$h_{NB} = C \Delta T_w^n \quad (5)$$

where C and n are constants taken from the heat transfer coefficient curves in Fig. 3.4 (a) and (b) for HFE-7100 and water respectively.. For HFE-7100, the power law was fit to only the 3 lowest heat flux points shown in Fig. 3.4(a). This was required due to the extremely vertical nature of the curve at higher nucleate boiling heat fluxes, even resulting in a slight reduction in superheat as heat flux increases.

Water has significant hookback, with higher heat fluxes occurring at a reduced superheat, as shown in Fig. 3.4(b). This is believed to be from surface effects resulting from the additive manufacturing process. The power correlation for water ignored the hookback points, using only data prior to the hookback. For easier viewing, the water hookback points are removed from all other boiling curves.

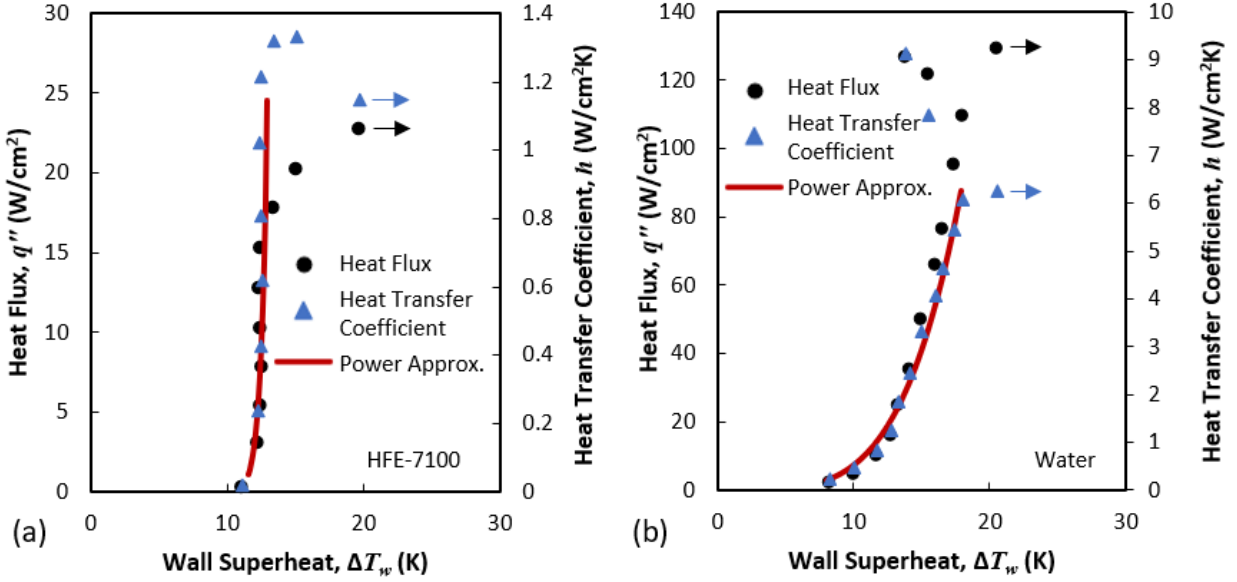


Fig. 3.4: Heat flux and heat transfer coefficient as a function of superheat for (a) HFE-7100 and (b) Water. The power approximation is the correlation used to estimate the nucleate boiling regime heat transfer coefficient as a function of superheat.

The natural convection regime was defined using correlations for a flat plate [39].

$$h_{NC} = 0.54k_l \left(\frac{g\beta\Delta T_w}{\nu\alpha L_b} \right)^{0.25} \quad (6)$$

where k_l is the thermal conductivity of the liquid, α is the thermal diffusivity of the liquid, ν is the kinematic viscosity of the liquid, and β is the expansion coefficient of the fluid. All properties are taken at the saturation conditions and assumed to be constant. The heat transfer coefficient was assumed to be zero at superheats below zero and the maximum natural convection superheat was determined by finding the intersection between Equation (6) and Equation (5).

Film boiling was defined using Zuber's film boiling correlation [40]:

$$h_{film} = \frac{h_{max}}{\left(\frac{\rho_l + \rho_v}{\rho_v} \right)} \quad (7)$$

where h_{max} is the heat transfer coefficient at the last point before CHF of the flat surface, marked with a horizontal arrow in Fig. 3.4(a) and (b). The superheat ΔT_{max} resulting in h_{max} was taken from

the power correlation given in Equation (5a) or (5b).. The film boiling heat transfer coefficient for a flat plate described in [41] was used to determine the superheat ΔT_{min} where film boiling begins.

$$h_{min} = 0.425 \left(\frac{k_v^3 h_{fg} \rho_v g (\rho_l - \rho_v)}{\mu_v \Delta T_w L_b} \right)^{0.25} \quad (8)$$

where k_v is the thermal conductivity of the vapor, h_{fg} is the latent heat of the fluid, and μ_v is the dynamic viscosity of the vapor. By finding the intersection of Equation (7) with Equation (8), the film boiling superheat, ΔT_{min} , required for film boiling as well as the heat transfer coefficient at that point can be determined. With the two points ΔT_{max} and ΔT_{min} defined and shown in Fig. 3.5(a) and (b), the regime between nucleate boiling and film boiling known as transitional boiling can be described. This was assumed to be a straight line, following the analysis of [17].

$$h_{trans} = \frac{h_{min} - h_{max}}{\Delta T_{min} - \Delta T_{max}} (\Delta T_w - \Delta T_{max}) \quad (9)$$

The full $h(\Delta T_w)$ function is plotted in Fig. 3.5(a) for HFE-7100 and Fig. 3.5(b) for water. Once this function is known, a set of governing energy balance equations for all segments and the boundary conditions is developed. This is then iteratively solved starting from an initial, constant fin temperature to determine the final temperature profile in each fin. The function $h(\Delta T_w)$ is then used with the temperature profile to calculate the total heat dissipated by the fin.

$$q_{fin} = \sum_{w=0}^{w=L} 2 \Delta T_w h(\Delta T_w) (L + t) dw \quad (10)$$

where L is the width of the fin, 20 mm. The same heat transfer was assumed through each fin in the sample, enabling predictions of the total heat flux dissipated by the heat sink.

$$q''_{tot} = \frac{q_{fin} N_{fin} + h(\Delta T_b) \Delta T_b A_{space} N_{space}}{A_{base}} \quad (11)$$

where N_{fin} is the number of fins, N_{space} is the number of spaces, ΔT_b is the known superheat at the base of the fins, A_{space} is the area of the spaces between fins, and A_{base} is the base footprint of the sample, 20×20 mm.

The resulting q''_{tot} in Equation (11) allows predictions of the boiling curves for various heat sink dimensions. By comparing predictions with the experimental boiling curve results for finned heat sinks, the key fin space and height length scales where the predictions hold accurate is determined.

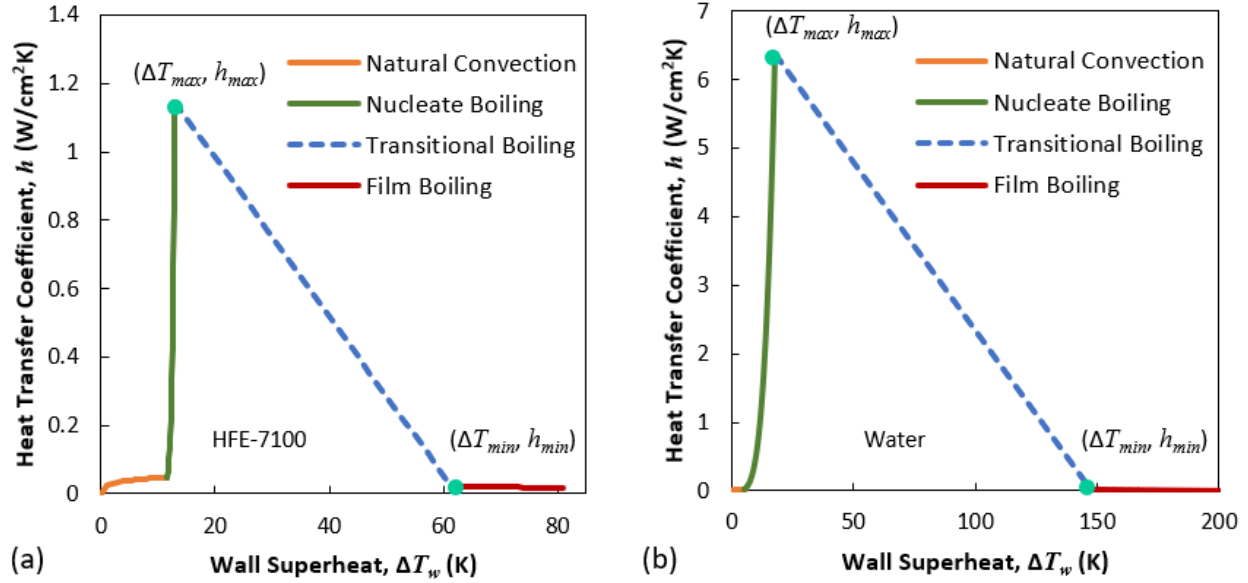


Fig. 3.5: $h(\Delta T_w)$ functions from a flat surface used in the predictions (a) HFE-7100 (b) Water. Points marked with a green dot show the points used to define the transitional boiling regime.

4. RESULTS AND DISCUSSION

4.1 Boiling Visualizations

High-speed visualizations are used to identify the boiling regimes and determine the heat fluxes where there was a boiling regime shift in all the tests. In the figures below, each photograph is a still image taken from a high-speed video, with a sketch below to highlight the key flow morphologies used to determine the regimes. The goal was not to draw every bubble accurately from the individual photo frame, but rather to convey what was occurring in the video. Overall, three regimes were observed at the base of the fins: uniform nucleate boiling, partial film boiling, and full film boiling. It should be noted that as heat flux increases and spacing decreases, it becomes increasingly difficult to visualize individual bubbles between the fins. Particularly for samples where $S=1.0$ mm, there is little backlight penetration between the fins and vapor billows in front of the fins, obscuring the camera view. As a result, the lowest and highest heat fluxes recorded for each regime may be slightly different than indicated.

The visual data from HFE-7100 for samples with $H=2.5$ are shown in Fig. 4.1. For all three samples, the top image represents the highest heat flux with uniform base nucleate boiling, while the bottom image is the lowest heat flux sustaining full base film boiling. The middle image is the partial film boiling regime, at a heat flux midway between the nucleate boiling and film boiling base regimes. Although the different regimes are easier to discern from vapor motion in videos, the change in bubble dynamics is quite clear. In the base nucleate boiling regime, all the bubbles are similarly sized, distributed uniformly across the entire base, and there are bubbles along the whole fin height, as shown in the top images of 4.1 (a) and (b). When the spacing is only 1.0 mm, the same order as the L_b of HFE-7100, there are still small and uniform bubbles between the fins, but there are also larger bubbles at the top of the fins. This is evidence of some type of confinement causing the small bubbles to coalesce.

The partial base film boiling regime, captured in the center row of images of Fig. 4.1, is identifiable due to the larger bubbles between the fins. They are no longer uniform, with some spaces being nearly covered in vapor and others with individual bubbles. A vapor layer is clearly forming between the fins. As boiling continues, the location of the forming vapor layer changes because as different portions of the heat sink are cooled by the individual bubbles, heat from the

vapor- covered sections can conduct to the slightly cooler areas, leading to a change in bubble/film location.

The full base film boiling regime appears quite similar between 4.1(a), (b), and (c) for different fin spacings. There is a clear layer of vapor completely covering the space between the fins. Higher up on the fins, there are smaller bubbles, preventing runaway CHF, though they are larger than in the nucleate boiling regime. One other point to note is that full base film boiling for H2.5-S8.5 and H2.5-S2.5 begins at $\sim 30 \text{ W/cm}^2$, near the CHF of the flat surface. This makes sense because the flat surface is in the film boiling condition at CHF. It is different for H2.5-S1.0, where full base film boiling develops at a heat flux over 15 W/cm^2 higher than for the flat surface. Moreover, H2.5-S1.0 did not develop full base film boiling until after a significant surface superheat increase and the temperature data began exhibiting unsteadiness. From this change in heat flux and surface temperature behavior, it is clear that full base film boiling behavior changes when $S=1.0 \text{ mm}$.

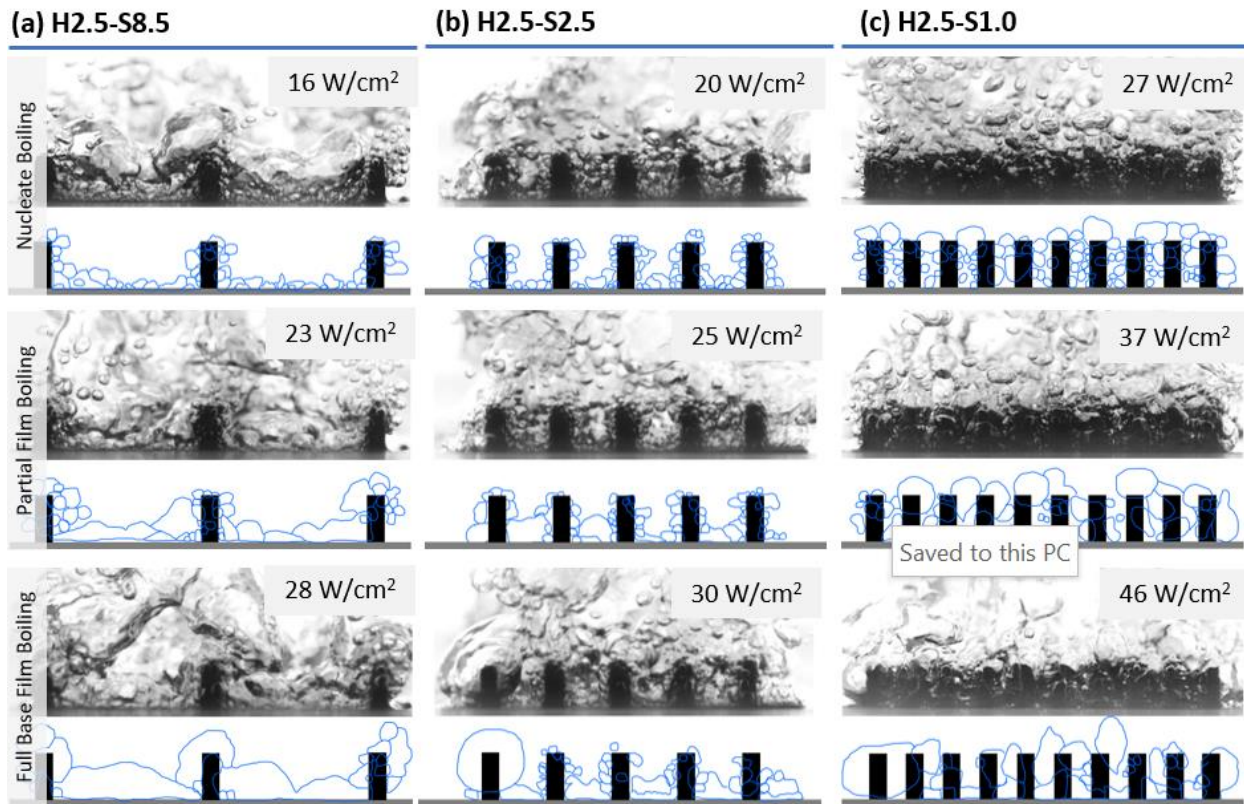


Fig. 4.1: Boiling regimes in HFE-7100 for 2.5 mm tall fins (a) H2.5-S8.5 (b) H2.5-S2.5 (c) H2.5-S1.0.

Fig. 4.2 shows samples where $H=8.5$ mm, much larger than the L_b of HFE-7100. The nucleate boiling regime is once again characterized by the small, uniform bubbles between the fin spaces while the partial base film boiling regime is denoted by large and small bubbles randomly distributed in varying locations. For H8.5-S1.0, the smallest spacing, full film boiling has a pulsing effect at high heat fluxes. Fig. 4.2(c) attempts to capture this by showing the small bubbles on the sides while a huge bubble envelops the center fins. The fins on the left have small, densely packed bubbles further up the fin while the fins on the right are mostly covered in vapor. This vapor moves across the sample in pulses, in an effect that appears similar to vapor instabilities in multiple flow boiling channels, when some channels are filled with vapor while others are nearly all fluid [42]. While this pulsing vapor effect was not seen for shorter fins, it further points to vapor confinement at 1.0 mm spacing. As spacing decreases from Fig. 4.2(a) to (b) to (c), it is also clear that the full base film boiling regime does not occur until higher heat fluxes. H8.5-S8.5 initiates full base film boiling at almost double the CHF of the flat surface, while H8.5-S1.0 develops full base film boiling at approximately four times the CHF of the flat surface. This sets these tallest fins apart from the other two heights.

For fins with $H=1.0$ mm on the same order as the L_b of HFE-7100, the nucleate boiling regime for all three spaces appears the same as the other two heights, as shown in the top row of Fig. 4.3. However, once the base partial film boiling regime is reached, all three samples have vapor almost entirely enveloping the short fins; there is not a separate film at the base with small bubbles at the top as was the case for taller fins. The full film boiling for all three samples occurred after a sudden large increase in superheat of around 20 K. Due to the short height, the vapor layer is not stable, and instead covers the fins, essentially provoking a gradual CHF condition. It should also be noted that the full film boiling condition developed at approximately the same heat flux for all three samples, $\sim 30 \text{ W/cm}^2$, again following the trends of the flat surface. Overall, these shortest samples show little heat flux enhancement compared to the flat surface.

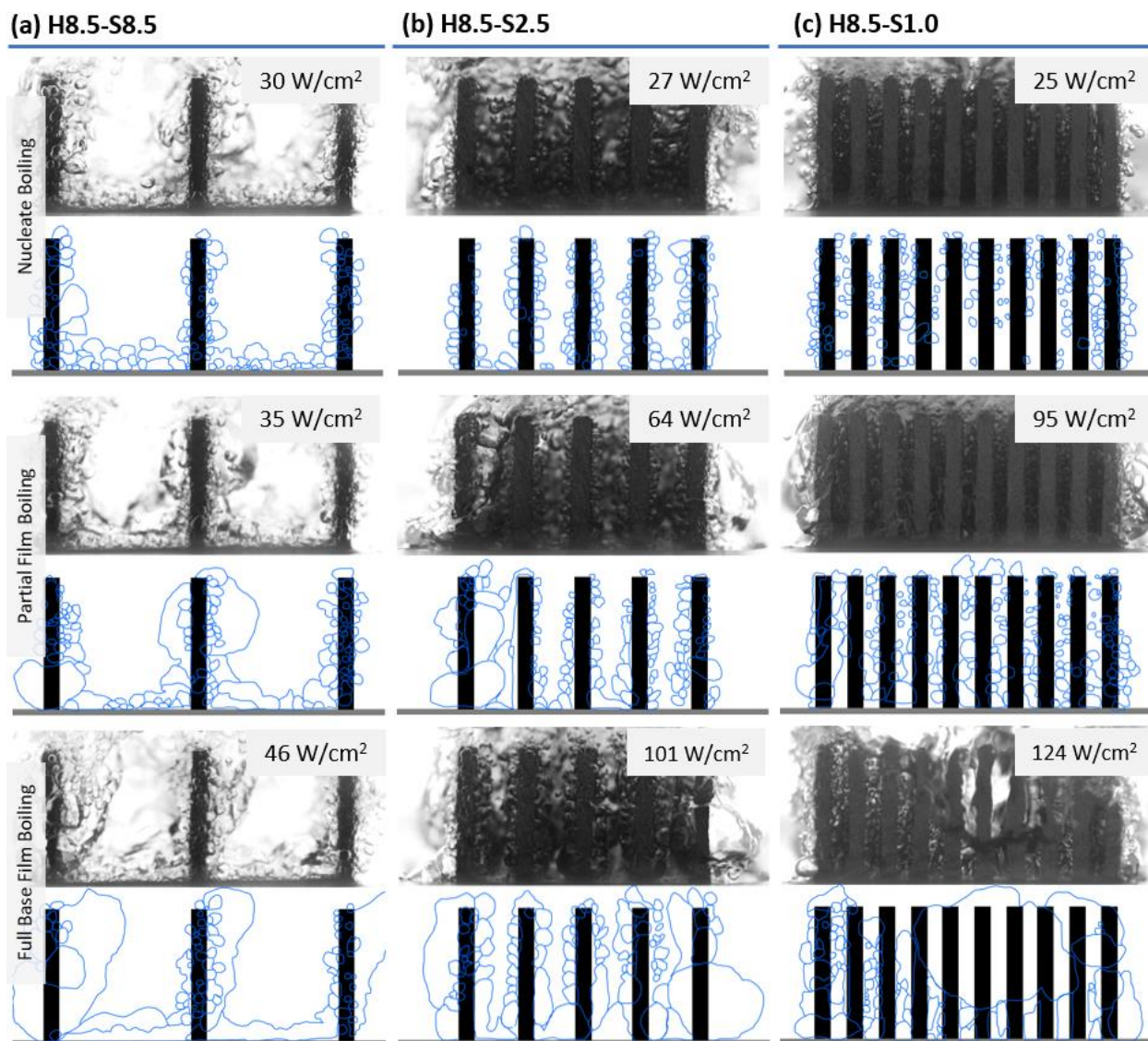


Fig. 4.2: Boiling regimes in HFE-7100 for 8.5 mm tall fins (a) H8.5-S8.5 (b) H8.5-S2.5 (c) H8.5-S1.0 .

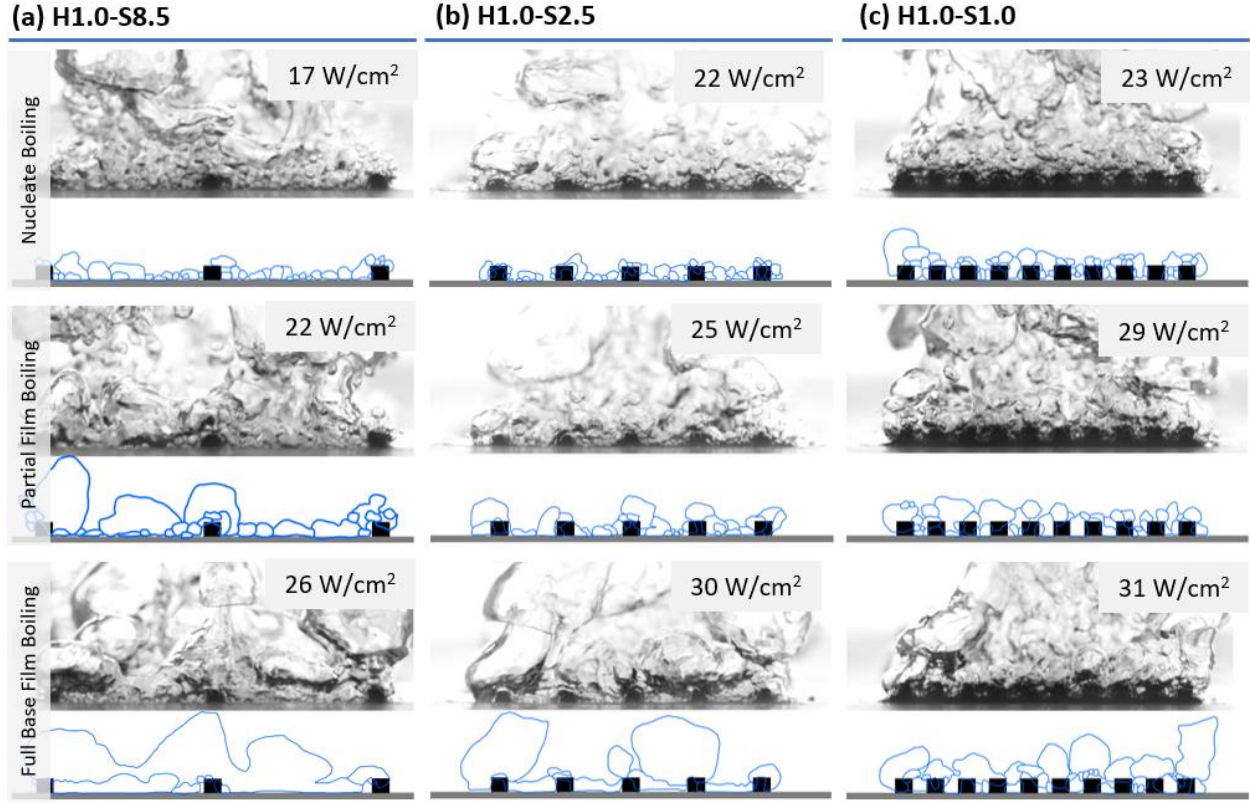


Fig. 4.3: Boiling regimes in HFE-7100 for 1.0 mm tall fins (a) H1.0-S8.5 (b) H1.0-S2.5 (c) H1.0-S1.0.

One last set of HFE-7100 visual data is shown in Fig. 4.4 for the H0.5-S0.5 sample. For this sample, both height and spacing are below the L_b of HFE-7100. Like the larger dimensioned samples above, the nucleate boiling regime in Fig. 4.4(a) is characterized by small bubbles uniformly covering the surface. While there is some indication of larger bubbles at the top of the sample indicating bubble confinement like for H2.5-S1.0 and H1.0-S1.0, it is less noticeable. Larger bubbles do not develop until the partial film boiling regime, shown in Fig. 4.4(b). The image is from the last point before CHF for this sample, and as for the 1.0 mm tall fins, some of the fins are starting to be covered in vapor. However, the sample never shows signs of developing a full film layer over the base only, and CHF transition occurred rapidly when compared to $H=1.0$ mm samples.

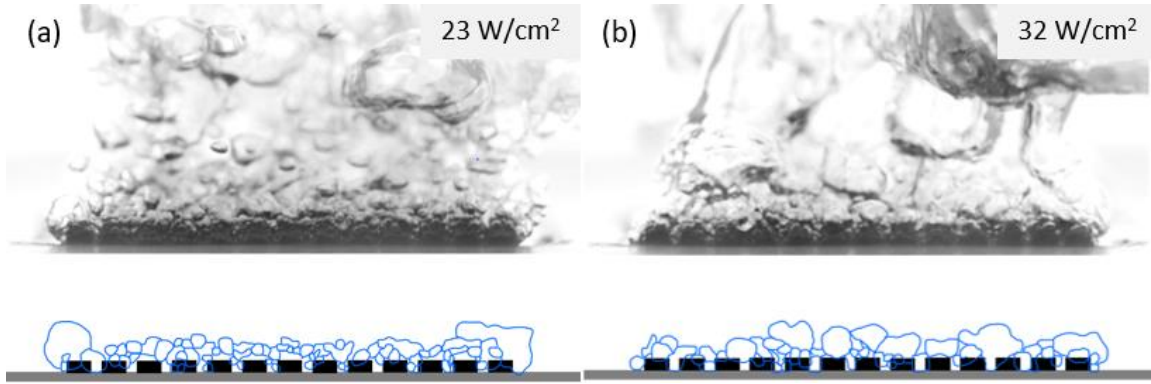


Fig. 4.4: Boiling regimes in HFE-7100 on H0.5-S0.5 (a) Nucleate boiling regime (b) Partial film boiling regime. Full film boiling was not reached before CHF.

To summarize, when the samples tested in HFE-7100 are compared, at close spacing $S=1.0$ mm, on the order of the capillary length, the full base film boiling regime consistently shifts to higher heat fluxes, apparently as a result from vapor confinement between the fins. Also, the smallest spacing has the largest number of fins, providing more area for bubble nucleation necessitating higher heat fluxes for vapor film layer development. Note that for short fins $H=1.0$ or 0.5 mm, the full base film boiling regime does not stabilize, and so the regime developing at higher heat fluxes is not evident. Because the larger $S=2.5$ and 8.5 mm spacings do not indicate the same increased heat flux requirements for fins where $H=2.5$ mm, and film boiling develops near the CHF film boiling condition on the flat surface, it is reasonable to assume that these fins are far enough apart to act independently of one another, and so can be described by the flat surface. When the fins are very tall, $H=8.5$ mm, there is slightly different behavior, even at 2.5 mm and 8.5 mm spacing. The full base film boiling regime requires higher heat fluxes for development for all 8.5 mm tall fins, but this effect seems to stem, not from vapor confinement, but from the high nucleation site density of these samples and amount of boiling area. There is a large sidewall area, and as can be seen in the visualizations, each fin has bubbles nucleating across this entire area. Because HFE-7100 is highly wetting and the additively manufactured surfaces are fairly rough, small, uniform bubbles can remain on the whole fin length until higher heat fluxes, delaying full base film boiling and CHF for $H=8.5$ mm. Effects from short fins in HFE-7100 are clear from the fact that the 1.0 mm and 0.5 mm tall fins do not develop a stable base full film boiling regime. Instead, even in the partial base film boiling regime, vapor is enveloping the fins, and ultimately there is little enhancement beyond the CHF of the flat surface.

Visualizations for water experiments were also analyzed. Samples with $H=8.5$ mm are shown to demonstrate the differences in the boiling regimes from the fluid change. Figure 4.5 has the same characteristic regimes as HFE-7100, though the specific boiling behaviors in each regime differ. The nucleate boiling regime is characterized by smaller bubbles nucleating at the base of the fins. However, for all spacings, the nucleation is only visible where the fins connect to the base surface. There is almost no boiling on the fin sidewalls. In Fig. 4.5(c), for $S=1.0$ mm, there is a change in appearance for the nucleate boiling regime. While the videos clearly show individual bubbles nucleating between the fins, there is also a lot of vapor billowing in front of them, such as is seen for other samples and HFE-7100 in the partial base film boiling regime. This is evidence of vapor entrapment due to the small spacing.

While the partial base film boiling and full base film boiling regimes for Fig. 4.5(a) and (b) also have the large vapor bubbles coming in front of the fins, all three samples have the vapor nucleating solely towards the base of the fins. As the vapor leaves the base surface, it clings to the fin sidewalls until departing off the tip. While the film layer of vapor does leave the surface in pulses, it is fairly uniform across the surface, and is vastly different from the channel effect seen in HFE-7100 for H8.5-S1.0. Even at low heat fluxes, the bubbles completely fill the space between the fins, except for cases when the spacing is much larger than the capillary length scale of water, $S=8.5$ mm.

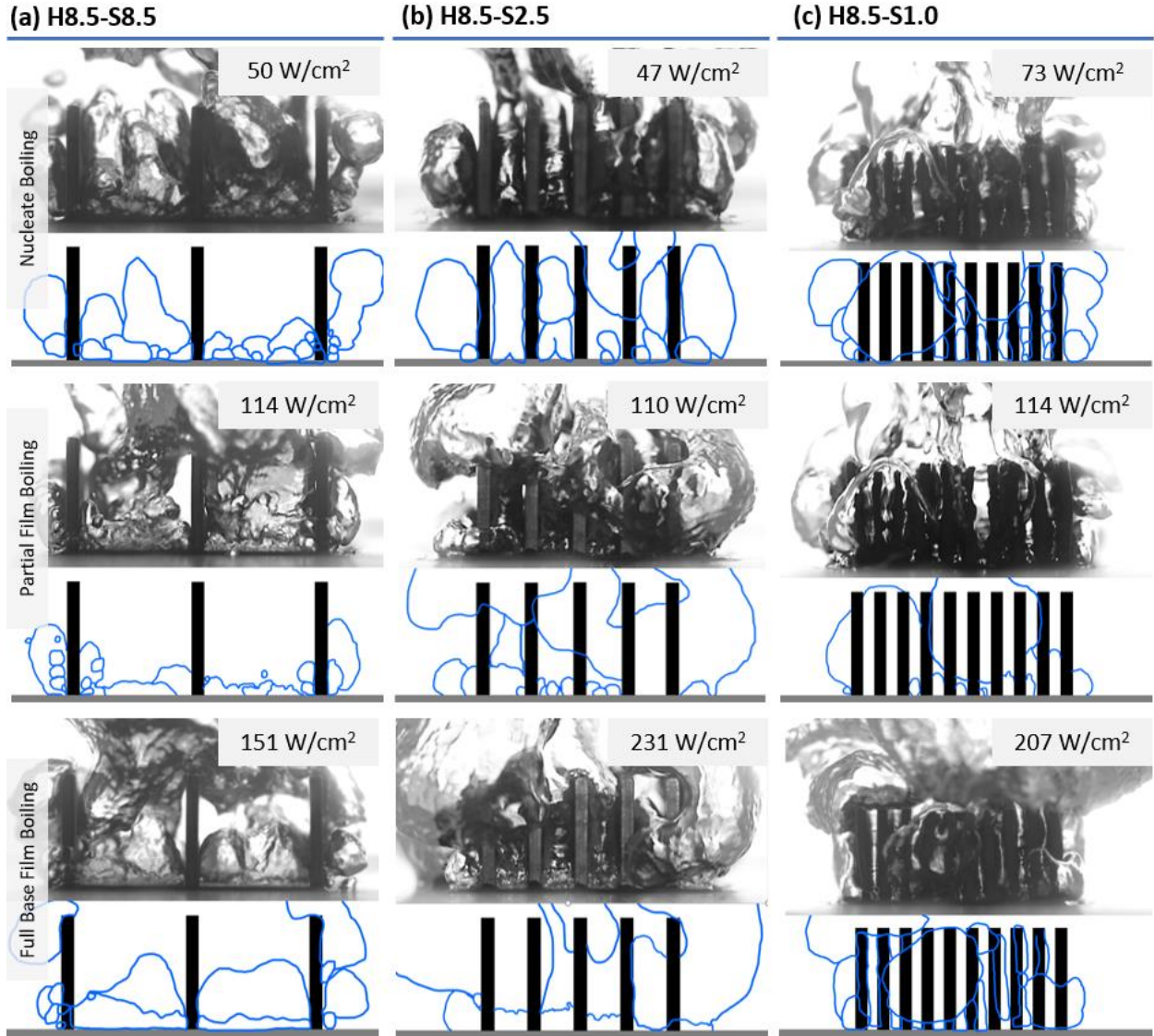


Fig. 4.5: Boiling regimes in water for 8.5 mm tall fins (a) H8.5-S8.5 (b) H8.5-S2.5 (c) H8.5-S1.0.

The flow visualization observations from water overall confirm the conclusions drawn from HFE-7100. There is clear evidence of bubble confinement for 1.0 mm spacing, below the capillary length scale, as evidenced by the huge amounts of vapor coming in front of the fins even in the nucleate boiling regime. Even at 2.5 mm spacing, on the order of the L_b of water, the bubbles seem slightly confined as they completely fill the spaces between the fins.

When heat fluxes are examined, the 1.0 mm spacing (smaller than the L_b of water) has the widest range of heat fluxes where bubbles are still individually nucleating at the base of the fins in the nucleate boiling regime. While higher heat fluxes are required for the development of the full base film boiling regime than for 8.5 mm spacing, the case when spacing is at the L_b of water develops the full base film boiling regime at the highest heat flux. This is most likely because there is too much vapor entrapment when $S < L_b$, leading to reduced heat transfer. The 1.0 mm spaced fins in water did not develop the channel-like instabilities seen in HFE-7100 for this spacing. One other observation is that the full base film boiling regime develops at significantly higher heat fluxes than the CHF of the flat surface for H8.5-S2.5 and H8.5-S1.0, further implying that the fins are not acting independently.

4.2 Boiling Curve Data

The experimental boiling curves are shown in the plots in this section, with the vertical axis showing heat flux defined from the base surface area, 20×20 mm. The horizontal axis is the superheat, ΔT_b , at the base of the fins. In the boiling curves, the regimes observed from the visualization data are reflected by the symbol shape. Diamonds denote the heat fluxes where there is uniform nucleate boiling across the base surface, circles are used for the sections of the boiling curve with the base of the sample in partial film boiling, and triangles show the portion of the curve where there is visually a full, stable film across the base of the surface between fins. Other annotations include arrows pointing to the right to denote CHF and filled symbols (versus open) to indicate when the data point was taken after a waiting period of 45 min, when it was clear that the strict steady state condition of <1K/hr change in surface temperature was not met. One other symbol, found only in HFE-7100 for the tallest fins, is a downward pointing arrow indicating when significant surface temperature oscillations around a steady value began.

4.2.1 Height Effects

The effects of fin height on the boiling curves are shown for HFE-7100 in Fig. 4.6 and water in Fig. 4.7. In order to focus solely on the height effects, a fixed spacing larger than the L_b of each fluid was chosen for the comparison across heights, while all curves are shown compared with the orange base surface boiling curve. In Fig. 4.6, the shortest fins where $H=1.0$ mm have a distinct behavior compared to the other two taller finned samples ($H=2.5$ mm and $H=8.5$ mm). The two taller sample have nearly identical boiling curves at low heat fluxes, matching the orange flat surface curve, until approximately at the CHF of the flat surface, $q'' = 20$ W/cm². After this point, the $H=8.5$ mm fins sustain higher heat fluxes at lower superheats, overall enhancing the CHF by almost five times that of the flat surface. The 2.5 mm tall fins still show marked improvement, with a CHF over 50% greater than that of the flat surface. In comparison, sample H1.0-S2.5 is further to the right and does not match the flat surface curve. Moreover, when $H=1.0$ mm, the fins reach CHF with less than 10% CHF enhancement when compared to the flat surface. H1.0-S2.5 did not achieve full base film boiling until after a significant temperature increase following CHF, overall indicating a significant indifference in boiling enhancement behavior for fins with height below the capillary length scale.

The boiling curves with water, as shown in Fig. 4.7, lead to the same height effect conclusions. All the curves are directly on top of the flat surface boiling curve, even more closely than HFE-7100, with the only differences occurring after the CHF of the flat surface. Both H2.5-S8.5 and H8.5-S8.5 were not run to CHF in water, but rather were stopped at the maximum 50 K superheat condition. However, it is still clear that increased height enables the extension of the boiling curves. The 1.0 mm tall fins have a marked difference from the taller fins. While the boiling curve still directly matches the flat surface curve, H1.0-S8.5 reaches essentially the same CHF as the flat surface and a film does not fully develop at the base of the fins before CHF. Because of how short the fins are, the full base film boiling regime cannot be sustained, and the fins provide little enhancement to the flat surface. Overall, if the fins are tall enough, fin height in both fluids does not affect the boiling curves at low heat fluxes, but increased height leads to improved heat transfer in the boiling curve at high heat fluxes above the CHF of the flat surface, verifying the observations of [19, 22, 30–32].

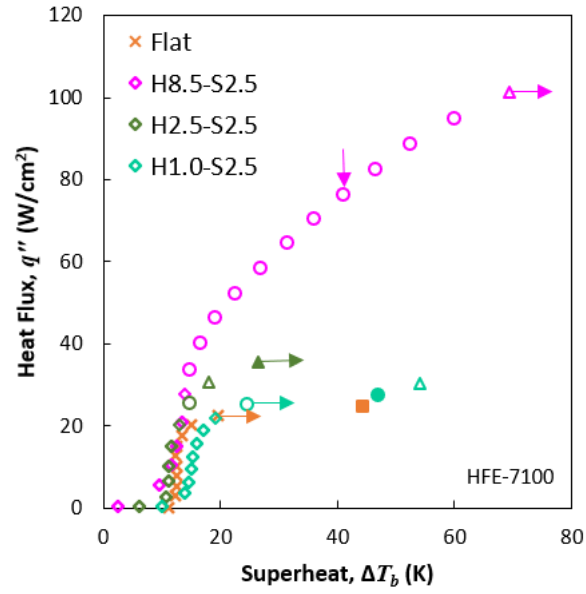


Fig. 4.6: Varying fin height in HFE-7100 at a constant 2.5 mm spacing.

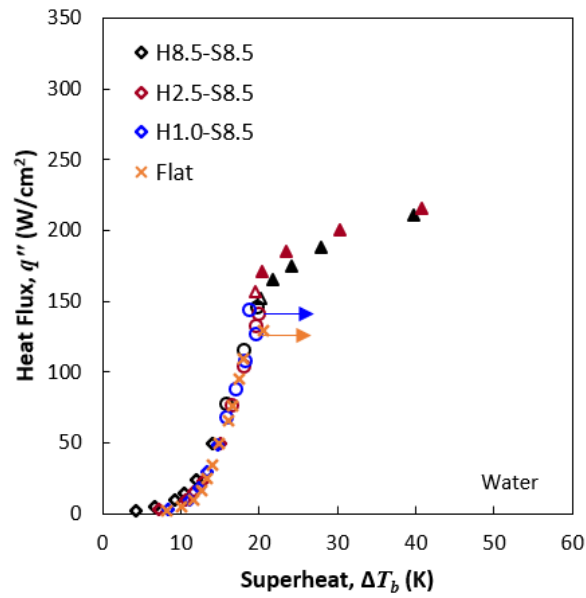


Fig. 4.7: Varying fin height in water at a constant 8.5 mm spacing.

4.2.2 Spacing Effects

Spacing effects for HFE-7100 are shown in Fig. 4.8 for spacings of (a) 8.5 mm, much larger than the L_b , and (b) 1.0 mm, on the same order as L_b . Looking at the HFE-7100 data for the larger $S=8.5$ mm, Fig. 4.8(a) has very similar boiling curves to Fig. 4.6; at low heat fluxes, the boiling curves lie on top of each other and the flat surface for the taller fins, while $H=1.0$ mm results in a curve with higher superheats at each heat flux. However, once the three heights are tested at $S=1.0$ mm, the L_b of HFE-7100, there is a clear change in the boiling curve trends, as shown in Figure 4.8(b). None of the finned boiling data lie directly on top of each other for any portion of the curve, and only H1.0-S1.0 lies on top of the flat surface. Height effects the entire boiling curve at this spacing, rather than just the heat fluxes above the CHF of the flat surface. When the boiling regimes are examined, there is a clear increase in superheat when entering the full base film boiling regime for samples with closer spacing, indicating confinement. H0.5-S0.5, with height and spacing below L_b , demonstrates further confinement effects through the changes to the entire boiling curve. The boiling curve is almost linear, demonstrating heat fluxes at lower superheats than the flat surface, and full base film boiling never develops. While H0.5-S0.5 slightly improves heat transfer performance compared to the flat surface, it is not due to supporting multiple boiling regimes.

Water demonstrates similar spacing effects to HFE-7100, with boiling curves shown in Fig. 4.9 as the spacing is varied from 8.5 to 2.5 to 1.0 mm. All three samples have $H=8.5$ mm, much larger than the L_b of water. Once again, the two larger spacings for this height have boiling curves that match the flat surface and each other. The most closely spaced H8.5-S1.0 sample, with spacing below the L_b of water, has a vastly different boiling curve compared to the larger spacings; it is almost linear in appearance. There is significant improvement in the heat transfer for the 1.0 mm spacing, with low heat fluxes at a decreased superheat than the other samples. Moreover, for H8.5-S1.0, the full base film layer develops at a significantly higher heat flux than the flat surface, clearly indicating that the fins do not act independently. One final observation is that when the full base film boiling regime develops in water, the surface temperature is no longer leveling to a steady value, as indicated by the filled symbols matching this regime for all samples. Remaining water boiling curves are given in Appendix B.

Both fluids show that varying boiling regimes leading to changes in slope in the curves for all samples. The initial nucleate boiling regime is the bottom half of the s-shaped curve, while the

upper half is started by the partial film boiling regime and finished by the base film boiling regime. These changes in slope make sense since the nucleate boiling regime is extremely efficient, with small increases in superheat leading to significantly increased heat fluxes. Once a film begins to develop, it insulates the surface, decreasing the efficiency of the heat transfer and increasing superheat for a given heat flux.

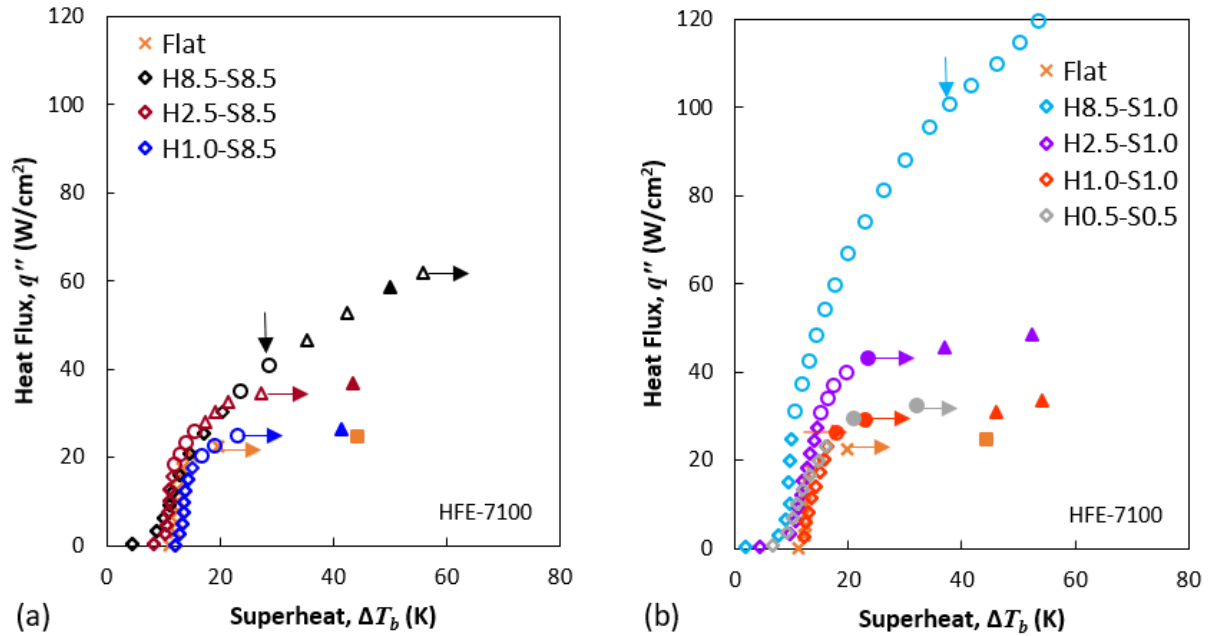


Fig. 4.8: Effects of spacing on fins in HFE-7100 (a) Spacing of 8.5 mm (b) Spacing of 1.0 mm and H0.5-S0.5

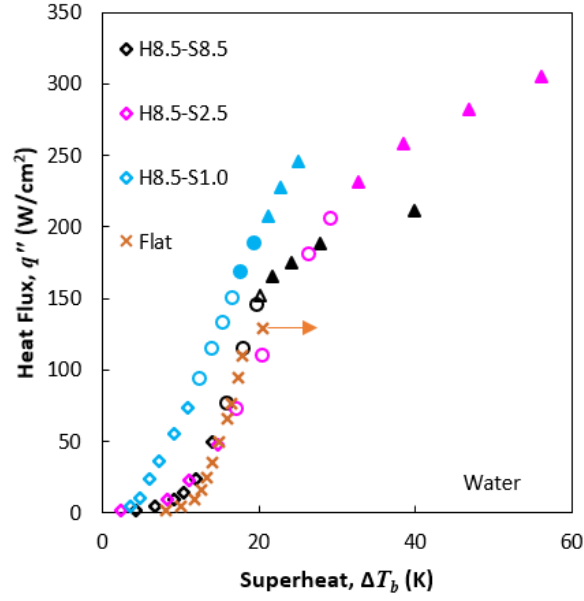


Fig. 4.9: Effects of spacing on fins in water, height at 8.5 mm with H2.5-S2.5 and H1.0-S1.0

4.2.3 Summary of Experimental Data

From the experimental data for HFE-7100, it is clear that when the fin height is at the capillary length scale L_b of the fluid, heat fluxes are at higher superheats compared to the heights above and below L_b . For spacings larger than L_b , the boiling curves are nearly identical at heat fluxes below the CHF of the flat surface, and changes in height and spacing only affect the heat fluxes above the CHF of the flat surface. Once spacing is at L_b , the low heat flux portion of the curves occur at lower superheats as height increases. When both height and spacing are below L_b , there is a more linear boiling curve with further decreased superheat at early heat fluxes compared to the flat surface.

Water verifies the height and spacing results well. Looking at spacing below the L_b of water, there is a significant decrease in superheat for all heat fluxes, and the small spacing leads to an almost linear boiling curve. Looking at height, for fins shorter than L_b , the sample went to CHF rather than sustaining base film boiling to the superheat ending condition. Because all tests for heights at or above L_b were unable to be run to CHF, conclusions cannot be made on taller fins outperforming shorter at either spacing. However, it is clear that there is a change between samples at the length scale of L_b versus smaller than L_b , both for height and spacing.

Examining the boiling regimes of the different samples for both fluids, when $H=8.5$ mm in HFE-7100 or all samples in water, the full base film boiling condition developed without the significant increases in superheat seen for short fins in HFE-7100. Smaller spacing for tall enough samples leads to lower superheats for heat fluxes as well as a higher heat flux requirement for full base film layer development. This information coupled with the confirmation from the visual data helps support why variable heat transfer coefficient is so important to consider when predicting boiling performance.

4.3 Boiling Superheat Predictions

Predictions of finned heat sink boiling performance were calculated for each of the samples to determine base superheat at each heat flux through the sample, following the approach described in Chapter 3.5. The key metrics for an accurate prediction are the CHF and the overall shape of the curve. CHF predictions are imperative to designing heat sinks for a specific heat load, and by capturing where the slope of the curve is changing, it will demonstrate that the flat surface can be used to predict the various boiling regimes. If the predictions match the experimental boiling results for a given heat sink, it will confirm that orientation of a surface in boiling does not affect the $h(\Delta T_w)$ function. Cases where predictions do not match will provide evidence of bubble confinement effects, showing where the fins no longer act independently and where the assumptions behind the predictions are no longer valid. Thus, the key length scales where fins can be described by a flat surface can then be determined.

4.3.1 HFE-7100 Predictions

Figure 4.10 provides an example of predicted versus experimental curve for H2.5-S8.5 in HFE-7100. As can be seen, there is a clear inflection point around 22 W/cm^2 in the prediction that matches where film boiling begins to dominate the base boiling behavior, and the slope continues to decrease until vapor covers the surface at CHF. The predictions are cut off at this point, where predicted heat flux is no longer increasing as base superheat increases. In order to better demonstrate the effectiveness of predictions between different samples, the predicted superheat at each heat flux is plotted in subsequent figures versus the experimental superheat at the base of the fins. Note that predictions were not available for experimental points at heat fluxes beyond the

predicted CHF, and no CHF points are indicated on the predicted versus experimental plots. Predicted CHF data is given in Chapter 4.3.3.

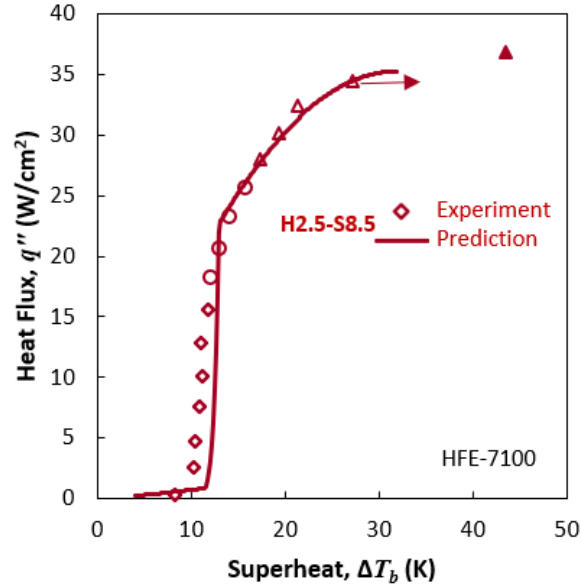


Fig. 4.10: Example of a boiling curve prediction for H2.5-S8.5 in HFE-7100.

For HFE-7100, Fig. 4.11(a) shows all the samples with height and spacing larger than the L_b of the fluid, while Fig. 4.11(b) is all the samples with spacing or height $\leq L_b$. According to the hypothesis, the predictions in Fig. 4.11(a) should be accurate throughout, while those in (b) at the same scale as L_b might not be as accurate due to bubble confinement effects. The prediction for H0.5-S0.5 should be incorrect as both height and spacing are smaller than L_b , and so the fins should not act independently.

Overall, the predictions in Fig. 4.11(a) support the hypothesis. Almost the entire nucleate boiling regime is captured by the predictions within $\pm 15\%$ for all samples, showing that the fins are tall enough and spaced far enough apart to act individually in this regime. H2.5-S8.5 is predicted particularly well throughout, through full base film boiling regime, while H2.5-S2.5 has good agreement until the highest superheats, both confirming that the assumptions for the predictions are reasonable. Looking at the 8.5 mm tall fins, the predictions are not within $\pm 15\%$ for the highest superheats in the nucleate boiling regime and all the points in the partial and full base film boiling regimes. However, even with the underpredicted superheats, there is still

evidence that the fins are acting independently since the predictions do not get worse at higher superheats; instead, the predicted versus experimental lines run parallel to the 45° line. The inaccuracies are most likely due to the large amount of sidewall nucleation not captured by the flat surface boiling behavior samples, as discussed in Chapter 4.1, though there could be further height confinement effects from the tall fins such as described by [19, 31].

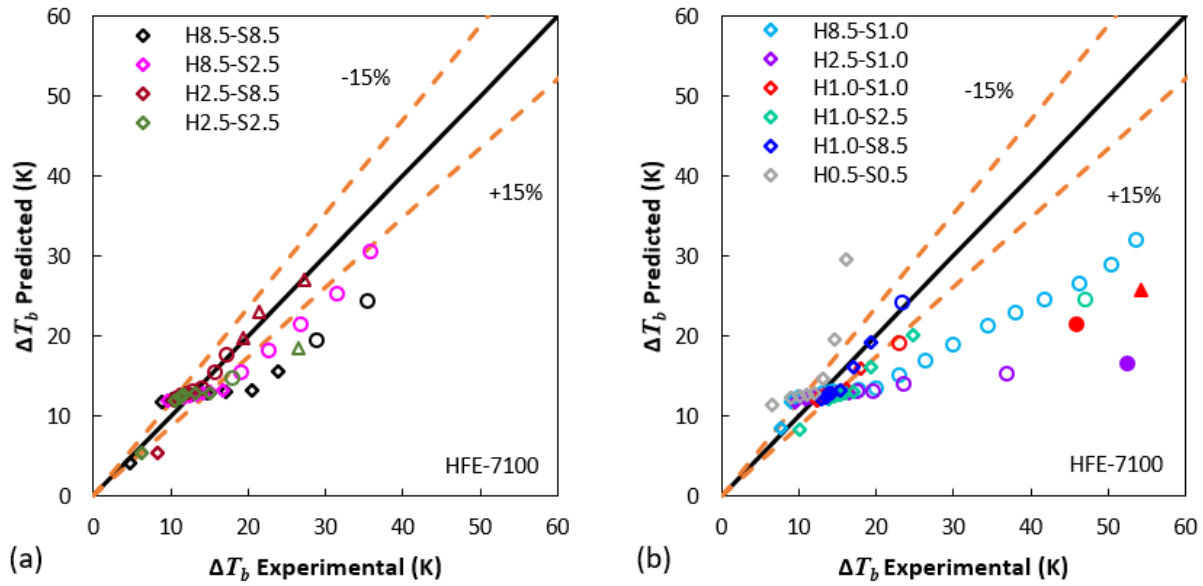


Fig. 4.11: Predicted superheat versus experimental superheats in HFE-7100 (a) Samples with both height and spacing above L_b (b) Samples with height or spacing at or below L_b .

Examining Fig. 4.11(b), it is clear that spacing is the dominant dimension for determining if the predictions are accurate. Heat sinks with $H=1.0$ mm are predicted within $\pm 15\%$ when the spacing is at 8.5 mm, though at smaller spacings, there is a decrease in accuracy at the highest superheats. Moreover, unlike the $H=8.5$ mm samples in Fig. 4.11(a), these high superheat points divert more and more from the 45° line, indicating that the heat sinks cannot be described by the flat surface. For H8.5-S1.0 and H2.5-S1.0, there is further confirmation of bubble confinement and the fins not acting independently. Outside the nucleate boiling regime, these samples are not well predicted, and the predictions are worse with increasing superheat. Lastly, the H0.5-S0.5 sample is not captured well by the predictions, even in the nucleate boiling regime. The superheat is

consistently over predicted and diverts further away from the 45° line as superheat increases. It is clear that spacing must be larger than L_b for accurate predictions, confirming the hypothesis.

4.3.2 Water Predictions

Predictions for boiling from heat sinks in water are shown in Fig. 4.12(a) and (b). Examining Fig. 4.12(a), where samples with both dimensions at or above the L_b of water are shown, it is clear that the hypothesis is further confirmed. In general, all boiling regimes are described by the predictions within $\pm 15\%$ until the filled points where base superheat was not converging to a steady value. While H8.5-S2.5 is not as well predicted, the 2.5 mm spacing is right at the L_b of water, and so the smaller spacing could result in height confinement effects that inhibit predicting the performance by using the flat surface.

Samples with at least one dimension below the L_b of water are shown in Fig. 4.12(b). Once again, it is clear that spacing is the dominant dimension to determine if predictions are accurate. Particularly at lower superheats, there is less prediction-experimental agreement when $S=1.0$ mm. The lower superheats seen in the boiling curves are not captured by the predictions, and it is clear that the fins are not acting independently, but instead have bubble confinement. H1.0-S8.5 is well predicted within $\pm 15\%$ for the entire curve, indicating that the spacing is large enough for independent fins, confirming the observations in HFE-7100.

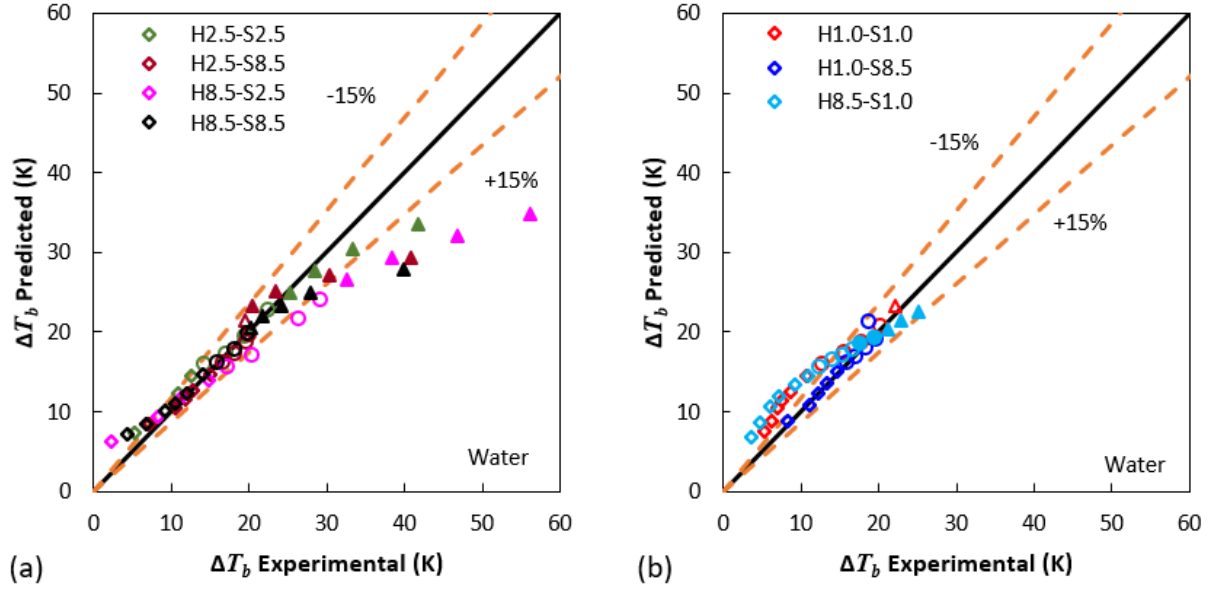


Fig. 4.12: Predicted superheat versus experimental superheats in HFE-7100 (a) Samples with both dimensions at or above L_b (b) Samples with height or spacing below L_b

4.3.3 CHF Predictions

Table 4.1 shows the experimental and predicted CHF values. Only samples that reached CHF are shown, with the top section for HFE-7100 and the bottom for water. The blue line between the HFE-7100 samples indicates where the samples transitioned from both dimensions larger than L_b to either dimension smaller than L_b .

In general, for HFE-7100, there is a trend of worsening CHF predictions as spacing decreases for a given height. Even for H2.5-S2.5, where both spacing and height are larger than L_b , there is still a difference greater than 15%. When $H=1.0$ mm, for $S=8.5$ mm and $S=2.5$ mm, the predicted CHF is within 15% of the experimental value. These two samples are very similar to the flat surface, with little enhancement, and so the predictions using the flat surface are accurate despite the fin height shorter than L_b . Once spacing is 1.0 mm, the CHF is significantly over predicted, most likely a result from the vapor enveloping the fins. H0.5-S0.5 has an under predicted CHF, probably because the short, closely spaced fins add additional enhancement similar to roughness that cannot be captured by the flat surface $h(\Delta T_w)$.

The two samples that reached CHF in water confirm the fact that fins below L_b cannot sustain multiple boiling regimes. The CHF is severely over predicted, and the relatively low experimental CHF indicates that the fins cannot continue into the full base film boiling regime, despite the predictions indicating otherwise. Instead, vapor covers the fins even at lower heat fluxes than the predictions would indicate, most likely because even in the partial base film boiling regime, there are already some fins fully covered in vapor, something not captured by the predictions which assume the fin sidewalls can be described by the flat surface.

Table 4.1: Experimental and Predicted CHF Values

HFE-7100			
Sample (Height-Spacing)	Experimental CHF (W/cm ²)	Predicted CHF (W/cm ²)	% Difference
H8.5-S8.5	61.6	52.6	15.8
H8.5-S2.5	101.0	72.7	32.6
H2.5-S8.5	34.4	35.3	2.6
H2.5-S2.5	35.5	43.7	20.7
H2.5-S1.0	42.9	64.8	40.7
H1.0-S8.5	24.7	26.1	5.5
H1.0-S2.5	24.9	28.5	13.5
H1.0-S1.0	28.9	34.4	17.4
H0.5-S0.5	32.0	23.2	31.9
Water			
Sample (Height-Spacing)	Experimental CHF (W/cm ²)	Predicted CHF (W/cm ²)	% Difference
H1.0-S8.5	142.8	298.5	70.6
H1.0-S1.0	194.4	396.8	68.5

4.4 Summary of Results

To summarize, the samples with both height and spacing above the L_b of the fluid act like independent fins and are accurately predicted using $h(\Delta T_w)$ from the flat surface. Visual data supports this with the evidence that fins spaced on the order of L_b have clear bubble confinement while fins on the same order as L_b are enveloped in vapor even in the partial film boiling regime. When spacing is below L_b , the boiling curves have lower superheats than the predictions would

indicate at low heat fluxes and the curve cannot be described using the behavior of the flat surface. It is clear that the fins do not act independently for these spacings. Height affects the higher heat fluxes of the boiling curve, with taller fins outperforming shorter. Fins in HFE-7100 with height at the L_b cannot sustain the full base film boiling regime, leading to increasingly inaccurate CHF predictions as spacing decreases. Fins in water confirm this, with the fins shorter than L_b resulting in significantly over predicted CHF. There also appears to be a maximum height in HFE-7100 where boiling performance differs from that of a flat surface, leading to predictions with an inaccuracy greater than 15%. However, for spacings that are larger than L_b , the assumption of independent fins still seems to be correct since the predictions do not divert as superheats increase. In general, spacing seems to be the more important dimension for determining if the flat surface can predict the fin performance, as is indicated by the decreasing CHF prediction accuracy with decreased spacing and the divergent predictions for samples with spacings at or below the L_b of HFE-7100. Overall, the hypothesis is well supported indicating that the independent fin assumption is only valid for fins with spacing larger than L_b and height at least on the same order as L_b .

5. CONCLUSIONS AND FUTURE WORK

5.1 Conclusions

The hypothesis is in general supported in all three sections of the results. From the visual data, it is clear that bubbles are confined for spacings below the L_b of the fluid. Larger bubbles emerging from the tops of the fins and billowing in front of the fins indicate that spacing at L_b is not sufficient for completely independent fins. Height effects show that for fins with $H=L_b$ have vapor enveloping the entire fin before a full, stable base film boiling regime develops, indicating a minimum height is required before the fins can improve heat transfer beyond the flat surface CHF.

Boiling curve data shows that fin spacing mostly affects the early part of the boiling curve while fin height changes the high heat flux performance. For both fluids, when spacing was below the L_b of the fluid, the low heat flux portion of the curves took on an almost linear appearance, with lower superheats overall. In HFE-7100, even for fins spaced at L_b there was a change in performance, with heat fluxes at slightly higher base superheats than larger spacings, implying that L_b is the key minimum length scale. At high heat fluxes in HFE-7100, taller fins resulted in higher performance for the same spacing. Water samples were in general not run to CHF, and so the late boiling curve performance could not be assessed. However, in both fluids, the shortest fins reached CHF before developing a stable full base film layer. For both fluids the differing behaviors when height or spacing is at L_b in HFE-7100 or below L_b in water indicate that L_b is the key length scale for individual fin behavior.

Lastly, predictions support the hypothesis. Spacing is the dominant dimension for accurate predictions, and fin spacing must be larger than L_b in HFE-7100 and at L_b in water for individual fin behavior and accurate predictions. When spacing is below this threshold, the predictions become increasingly inaccurate as superheat increases. Height effects are well captured by predictions in both fluids for all heights at or above L_b , though the final CHF predictions are increasingly underpredicted as spacing decreases. There also appears to be a maximum height after which the assumption that the fin sidewalls behave like a flat surface are not as accurate, though the individual fin assumption still holds. While this height threshold was not accounted for in the

hypothesis, it is possibly the result of the fin sidewalls being printed in a different orientation from the flat surface or the spaces between the fins.

The fact that predictions can capture the trends of boiling in two fluids with differing wettability and properties is itself a breakthrough. The capillary length L_b is the key length scale for bubble confinement in boiling, and care must be taken to ensure that proper dimensions are maintained, particularly for spacing, in order to correctly implement the assumption that all fins are individual with sides that can be described by the flat surface. More insight into maximum fin height is required, though overall, the single fin predictions of [24] can in fact be successfully applied to an array if both height and spacing are larger than L_b .

5.2 Future Work

Further analysis of fin dimensions would be invaluable to developing predictions when height and/or spacing is below L_b . The predictions in this thesis increasingly diverged with increasing superheat, particularly for spacings below L_b , but there may be a scaling method proportional to the spacing to account for the confinement effects. From the visualization in HFE-7100, incorporating channel flow boiling heat transfer correlations into $h(\Delta T_w)$ could account for the confinement effects. Similarly, providing a cutoff for fin performance predictions when the fins are shorter than L_b could enable predictions for a wider range of heights. The successful modeling of an increased range of dimensions would provide significant insight into confinement effects in boiling which would be applicable in other scenarios.

The additively manufactured surfaces are quite rough, and this clearly effects HFE-7100 more than water, as seen in the nucleation across the entire fin sidewall in the refrigerant at even low heat fluxes. The fact that predictions derived from the additively manufactured flat surface apply to the fin arrays implies that other surface enhancements could be incorporated into predictions as well. Varying wettability, nanostructures, and other enhancements could be tested on a flat surface first to obtain the nucleate boiling portion of the $h(\Delta T_w)$ function. This function could then be applied to a fin array to predict the micro-scale enhanced heat sink. It would be necessary to verify minimum length scales for fin independence in order to incorporate the fundamental assumption that the flat surface can be used to describe the structure behavior. If this is the case, predictions could be developed for multi-scale enhanced heat sinks for extreme heat flux dissipation.

Observations on orientation effects can also be made from these experiments. Since the horizontal flat surface boiling performance can be used to predict the vertical fin sidewall, it is likely that orientation does not matter, so long as the fins can still be treated as individual. Verification of this would provide confidence to implementing boiling heat sinks into large scale immersion cooling applications which often have vertical heated surfaces rather than the horizontal tested here.

With the orientation question is the question of shadowing, when bubbles from a lower heat source flow past a higher heat source. This would be seen in practical implementation of immersion cooling in a data center, when multiple computer processing units are placed one above the other in a tank. Will predictions using a flat surface $h(\Delta T_w)$ function still be accurate if vapor from one heat sink flows past another heat sink before being condensed? There is the possibility of bubble confinement from the additional vapor from another source.

The orientation and shadowing research are key to designing topology optimized surfaces. Developed by iteratively optimizing the heat transfer at each point in the heat sink, these surfaces often have branched structures that point in different directions at in the bubble path of other structures. Before boiling performance predictions for these heat sinks can be developed, it is necessary to determine if a flat surface $h(\Delta T_w)$ function can still be applied at each point. Moreover, features are not always completely smooth or regular, possibly further impacting the effectiveness of a prediction developed using a flat surface. Feature length scales such as minimum radius of curvature in a heat sink component or spacing between small features must also be considered. It may also be possible to predict the best optimized heat sink design with simplifying assumptions such as no bubble confinement and an average heat transfer coefficient, but predicting the CHF or superheat at a given heat flux would be nearly impossible without the variable heat transfer coefficient being implemented.

APPENDIX A. VERIFYING POOL BOILING CONDITIONS

Boiling experiments on a flat, machined copper block were performed in water at vastly different flow rates into the plenum of ~175 mL/min and ~530 mL/min, as shown in Fig. A1. The data match, indicating both the repeatability of tests and that flow rates are sufficiently small that they do not impact the performance of the sample and the sample is in pool boiling conditions (versus flow boiling).

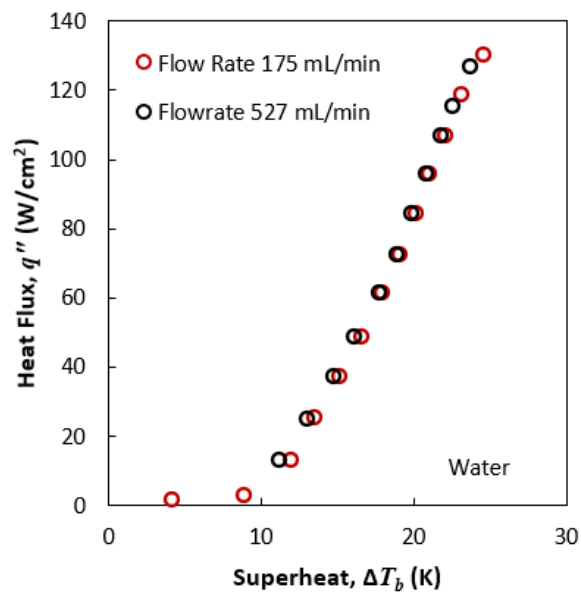


Fig. A1: Water pool boiling curves for a machined flat surface at two different flow rates.

Experiments on additively manufactured flat surfaces were also performed at different flow rates in HFE-7100. The change in flow rate is lesser than the confirmation of pool boiling during water tests, but the results in Fig. A2 still clearly shows excellent repeatability under these conditions, and indicate the pool boiling condition.

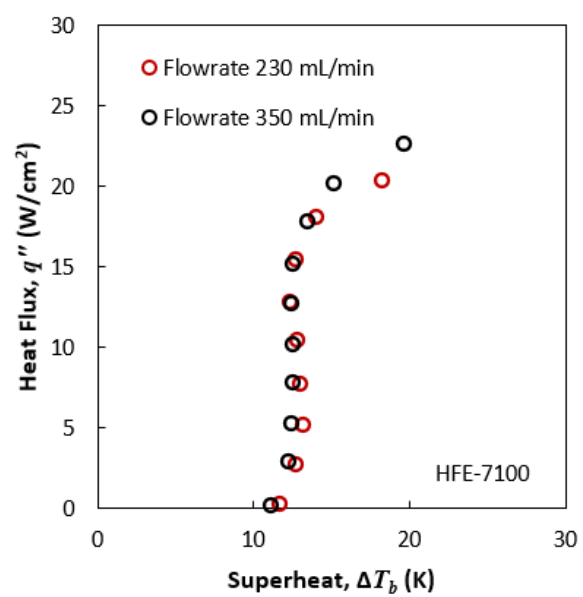


Fig. A2: HFE-7100 pool boiling curves for an additively manufactured flat surface at two different flow rates.

APPENDIX B. REMAINING WATER BOILING CURVES

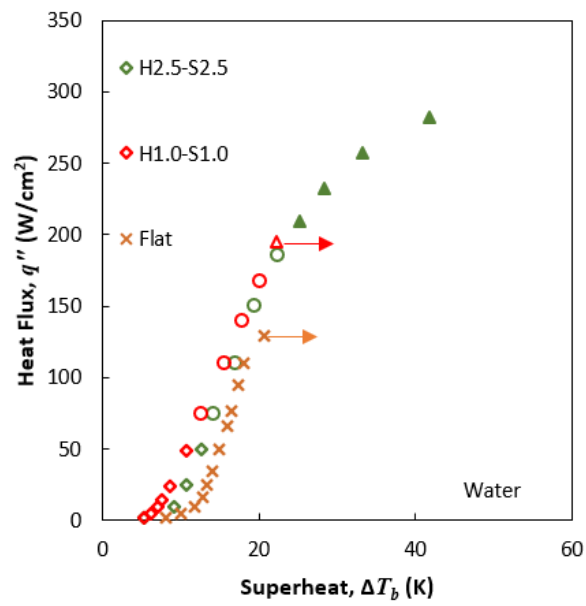


Fig. B1: Boiling curves for H1.0-S1.0 and H2.5-S2.5 in water.

REFERENCES

- [1] X. Yuan, X. Zhou, Y. Pan, R. Kosonen, H. Cai, Y. Gao, and Y. Wang., “Phase change cooling in data centers: A review,” *Energy Build.*, vol. 236, p. 110764, 2021.
- [2] X. Gong, Z. Zhang, S. Gan, B. Niu, L. Yang, H. Xu, and M. Gao, “A review on evaluation metrics of thermal performance in data centers,” *Build. Environ.*, vol. 177, p. 106907, 2020.
- [3] M.-G. Kang, “Effect of surface roughness on pool boiling heat transfer,” *Int. J. Heat Mass Transf.*, vol. 43, no. 22, pp. 4073–4085, Nov. 2000.
- [4] B. J. Jones, J. P. McHale, and S. V. Garimella, “The influence of surface roughness on nucleate pool boiling heat transfer,” *J. Heat Transf.*, vol. 131, no. 12, p. 121009, 2009.
- [5] C. M. Kruse, T. Anderson, C. Wilson, C. Zuhlke, D. Alexander, G. Gogos, and S. Ndao, “Enhanced pool-boiling heat transfer and critical heat flux on femtosecond laser processed stainless steel surfaces,” *Int. J. Heat Mass Transf.*, vol. 82, pp. 109–116, 2015.
- [6] T. P. Allred, J. A. Weibel, and S. V. Garimella, “Enabling highly effective boiling from superhydrophobic surfaces,” *Phys. Rev. Lett.*, vol. 120, no. 17, p. 174501, 2018.
- [7] A. R. Motezakker, A. K. Sadaghiani, S. Çelik, T. Larsen, L. G. Villanueva, and A. Koşar, “Optimum ratio of hydrophobic to hydrophilic areas of biphilic surfaces in thermal fluid systems involving boiling,” *Int. J. Heat Mass Transf.*, vol. 135, pp. 164–174, 2019.
- [8] K. Ferjančič, M. Može, P. Križan, M. Bobič, and I. Golobič, “Subcooled critical heat flux on laser-textured stainless-steel ribbon heaters in pool boiling of FC-72,” *Int. J. Heat Mass Transf.*, vol. 159, p. 120090, 2020.
- [9] T. P. Allred, J. A. Weibel, and S. V. Garimella, “The petal effect of parahydrophobic surfaces offers low receding contact angles that promote effective boiling,” *Int. J. Heat Mass Transf.*, vol. 135, pp. 403–412, 2019.
- [10] S. G. Liter and M. Kaviani, “Pool-boiling CHF enhancement by modulated porous-layer coating: theory and experiment,” *Int. J. Heat Mass Transf.*, vol. 44, no. 22, pp. 4287–4311, 2001.
- [11] S. Sarangi, J. A. Weibel, and S. V. Garimella, “Quantitative evaluation of the dependence of pool boiling heat transfer enhancement on sintered particle coating characteristics,” *J. Heat Transf.*, vol. 139, no. 2, p. 021502, 2016.
- [12] G. Liang and I. Mudawar, “Review of nanoscale boiling enhancement techniques and proposed systematic testing strategy to ensure cooling reliability and repeatability,” *Appl. Therm. Eng.*, vol. 184, p. 115982, 2021.

- [13] S. Bhavnani, V. Narayanan, W. Qu, M. Jensen, S. Kandlikar, J. Kim, and J. Thome, “Boiling augmentation with micro/nanostructured surfaces: Current status and research outlook,” *Nanoscale Microscale Thermophys. Eng.*, vol. 18, no. 3, pp. 197–222, 2014.
- [14] U. Sajjad, A. Sadeghianjahromi, H. M. Ali, and C.-C. Wang, “Enhanced pool boiling of dielectric and highly wetting liquids – A review on surface engineering,” *Appl. Therm. Eng.*, vol. 195, p. 117074, 2021.
- [15] G. Liang and I. Mudawar, “Review of pool boiling enhancement by surface modification,” *Int. J. Heat Mass Transf.*, vol. 128, pp. 892–933, 2019.
- [16] W. Li, R. Dai, M. Zeng, and Q. Wang, “Review of two types of surface modification on pool boiling enhancement: Passive and active,” *Renew. Sustain. Energy Rev.*, vol. 130, p. 109926, 2020.
- [17] N. Abuaf, S. H. Black, and F. W. Staub, “Pool boiling performance of finned surfaces in R-113,” *Int. J. Heat Fluid Flow*, vol. 6, no. 1, pp. 23–30, 1985.
- [18] F.-S. Lai and Y.-Y. Hsu, “Temperature distribution in a fin partially cooled by nucleate boiling,” *AIChE J.*, vol. 13, no. 4, pp. 817–821, 1967.
- [19] K. N. Rainey and S. M. You, “Pool boiling heat transfer from plain and microporous, square pin-finned surfaces in saturated FC-72,” *J. Heat Transf.*, vol. 122, no. 3, pp. 509–516, 2000.
- [20] D. R. Cash, G. J. Klein, and J. W. Westwater, “Approximate optimum fin design for boiling heat transfer,” *J. Heat Transf.*, vol. 93, no. 1, pp. 19–23, 1971.
- [21] C. Beurtheret, “L’ébullition à flux imposé sur paroi non isotherme,” *Journ. Hydraul.*, vol. 7, no. 1, pp. 118–126, 1963.
- [22] I. Mudawar and T. M. Anderson, “Optimization of enhanced surfaces for high flux chip cooling by pool boiling,” *J. Electron. Packag.*, vol. 115, no. 1, pp. 89–100, 1993.
- [23] I. Mudawar and T. M. Anderson, “Parametric investigation into the effects of pressure, subcooling, surface augmentation and choice of coolant on pool boiling in the design of cooling systems for high-power-density electronic chips,” *J. Electron. Packag.*, vol. 112, no. 4, pp. 375–382, 1990.
- [24] K. W. Haley and J. W. Westwater, “Boiling heat transfer from single fins,” in *The 3rd International Heat Transfer Conference (IHTC)*, 1966.
- [25] W. W. Lin and D. J. Lee, “Boiling on a straight pin fin,” *AIChE J.*, vol. 42, no. 10, pp. 2721–2728, 1996.
- [26] F. Fantozzi, A. Franco, and E. M. Latrofa, “Analysis of the heat dissipation enhancement with finned surfaces in pool boiling of dielectric fluid,” *Heat Mass Transf.*, vol. 36, no. 6, pp. 487–495, 2000.

- [27] T. M. Anderson and I. Mudawar, "Microelectronic cooling by enhanced pool boiling of a dielectric fluorocarbon liquid," *J. Heat Transf.*, vol. 111, no. 3, pp. 752–759, 1989.
- [28] N. Zuber, "Hydrodynamic aspects of boiling heat transfer," *Dr. Diss. Univ. Calif.*, 1959.
- [29] G. Guglielmini, M. Misale, and C. Schenone, "Experiments on pool boiling of a dielectric fluid on extended surfaces," *Int. Commun. Heat Mass Transf.*, vol. 23, no. 4, pp. 451–462, 1996.
- [30] G. J. Klein and J. W. Westwater, "Heat transfer from multiple spines to boiling liquids," *AIChE J.*, vol. 17, no. 5, pp. 1050–1056, 1971.
- [31] C. K. Yu and D. C. Lu, "Pool boiling heat transfer on horizontal rectangular fin array in saturated FC-72," *Int. J. Heat Mass Transf.*, vol. 50, no. 17–18, pp. 3624–3637, 2007.
- [32] W. R. McGillis, V. P. Carey, J. S. Fitch, and W. R. Hamburg, "Pool boiling enhancement techniques for water at low pressure," in *The 7th IEEE Semiconductor Thermal Measurement and Management Symposium*, pp. 64–72 1991.
- [33] K.-A. Park and A. E. Bergles, "Boiling heat transfer characteristics of simulated microelectronic chips with detachable heat sinks," in *The 8th International Heat Transfer Conference (IHTC)*, 1986.
- [34] M. J. Rau and S. V. Garimella, "Local two-phase heat transfer from arrays of confined and submerged impinging jets," *Int. J. Heat Mass Transf.*, vol. 67, pp. 487–498, 2013.
- [35] C. Mira-Hernández, J. A. Weibel, and S. V. Garimella, "Visualizing near-wall two-phase flow morphology during confined and submerged jet impingement boiling to the point of critical heat flux," *Int. J. Heat Mass Transf.*, vol. 142, p. 118407, 2019.
- [36] M. D. Clark, J. A. Weibel, and S. V. Garimella, "Identification of nucleate boiling as the dominant heat transfer mechanism during confined two-phase jet impingement," *Int. J. Heat Mass Transf.*, vol. 128, pp. 1095–1101, 2019.
- [37] M. J. Rau and S. V. Garimella, "Confined jet impingement with boiling on a variety of enhanced surfaces," *J. Heat Transf.*, vol. 136, no. 10, p. 101503, 2014.
- [38] K. Brown, H. Coleman, and W. Steele, "Estimating uncertainty intervals for linear regression," in *The 33rd Aerospace Sciences Meeting and Exhibit*, 1995.
- [39] J. R. Lloyd and W. R. Moran, "Natural convection adjacent to horizontal surface of various planforms," *J. Heat Transf.*, vol. 96, no. 4, pp. 443–447, 1974.
- [40] N. Zuber, "On the stability of boiling heat transfer," *Trans. Am. Soc. Mech. Eng.*, vol. 80, no. 3, pp. 711–714, 1958.
- [41] P. J. Berenson, "Film-boiling heat transfer from a horizontal surface," *J. Heat Transf.*, vol. 83, no. 3, pp. 351–356, 1961.

- [42] Y. K. Prajapati and P. Bhandari, “Flow boiling instabilities in microchannels and their promising solutions – A review,” *Exp. Therm. Fluid Sci.*, vol. 88, pp. 576–593, 2017.